Improving the Quality of Subalpine Precipitation Measurements with Hydrometeor Information and a Hierarchical Bayesian Gauge Correction Model

by

J. Bryan Curtis

B.S., Humboldt State University, 2010

A thesis submitted to the

Faculty of the Graduate School of the

University of Colorado in partial fulfillment

of the requirement for the degree of

Master of Arts

Department of Geography

2019

This thesis entitled:
Improving the Quality of Subalpine Precipitation Measurements
with Hydrometeor Information and a
Hierarchical Bayesian Gauge Correction Model

Written by John Bryan Curtis

has been approved for the Department of Geography

by

_____
Peter Blanken

_____
Katja Friedrich

_____
Mark Serreze

Date _____

The final copy of this thesis has been examined by the signatories, and we find that both the content and the form meet acceptable presentation standards of scholarly work in the above mentioned discipline.

Curtis, John Bryan (M.A., Geography)

Improving the Quality of Subalpine Precipitation Measurements with Hydrometeor Information and a Hierarchical Bayesian Gauge Correction Model

Thesis directed by Professor Peter D. Blanken

Abstract

A Bayesian machine learning method was used to produce a skillful precipitation gauge correction for an unshielded gauge in the subalpine forest below Niwot Ridge, Colorado. A U.S. Climate Reference Network (USCRN) gauge provided the "true" reference precipitation accumulation from which a gauge correction was developed. The difference in daily precipitation between the USCRN gauge and the unshielded gauge, integral to a precipitation record extending back to 1952, was modelled using hydrometeor characteristics, wind speed, and precipitation intensity and duration. Probability distributions of explanatory variables were estimated and used as likelihood information for a hierarchical Bayesian regression gauge correction (HBayeRGC) model. The HBayeRGC explains 86% of the unshielded gauge errors during an October 2013 to May 2015 gauge comparison period and provides a novel method for estimating precipitation gauge uncertainties. Error-prone precipitation gauges in windy mountain environments can be corrected with the HBayeRGC to improve understanding of mountain water resources.

Contents

Chapter

List of Tables

List of Figures

Chapter 1

Introduction

Understanding the influence of climate change on the water cycle hinges on *accurate* and *precise* long-term observations of precipitation. Precipitation gauges, the only instruments directly measuring precipitation, suffer from substantial wind-induced errors if poorly shielded (Colli et al., 2016a, 2016b; Goodison et al., 1998; Rasmussen et al., 2011; Sevruk et al., 2009; Sugiura et al., 2006; Thériault et al., 2015). A standard method to correct for these errors is to apply a wind correction model that is derived from the differences between unshielded gauges and gauges with the World Meteorological Organization's standard wind shield, the Double Fence Intercomparison Reference (DFIR) (Chen et al., 2015; Kochendorfer et al., 2017a, 2018; Wolff et al., 2015; Yang et al., 1998a, 1998b, 1999). Since a wind correction algorithm strongly depends on hydrometeor type, including diameter and fall speed into the correction approach is a novel means to reduce wind-induced errors (Thériault et al., 2012). Equally important to accurate precipitation records is quantifying the uncertainty in accumulation. However, current gauge correction approaches miss the opportunity to estimate variable uncertainty, based

on the combination of all explanatory and unknown physical conditions, at the time scale of observation. The objectives of this thesis, is to further improve precipitation gauge corrections in error-prone complex terrain that specifically corrects an insufficiently shielded gauge in the Niwot Ridge, Colorado subalpine ecosystem with accurate reference precipitation data from a co-located DFIR gauge. To meet this objective, we develop a machine learning gauge correction model that includes hydrometeor, wind, and precipitation type and intensity predictor information. This novel approach provides meaningful uncertainty estimations for accumulated mountain precipitation and has the potential to improve our understanding of orographic precipitation patterns impacting precious water resources.

Large errors in precipitation measurement occur in mountain environments where high winds combine with frozen hydrometeors (i.e., snow) that are more susceptible to the influence of airflow around the gauge orifice (Colli et al., 2016a, 2016b; Thériault et al., 2012, 2015). Accurately-measured precipitation in subalpine and alpine zones is critical to understanding the role of orographic enhancement of precipitation over mountain catchments that ultimately contribute significantly to water resources (75% of surface- and groundwater supplies in the Western United States, IPCC 2007). Unfortunately, the spatial gaps in mountain precipitation observations are larger than the ~1 km resolution required for mountain catchment hydrological models (Bales et al., 2006) with gauges generally located in protected sites (e.g. forest clearings and gaps) that may or may not represent local average conditions (Strachan et al., 2016). This specifically contributes to gaps in direct observations of mountain snow-atmosphere interactions

(Lehning et al., 2008; Mott et al., 2014) and necessitates high-quality data from gauges currently in operation. To understand the role of mountain precipitation in a changing climate, such as the effect that decreasing 700 mb winds in the Western United States have on orographic precipitation (Dettinger, 2014), multi-decade precipitation gauge records in mountain environments need to be corrected for under- and overcatchment errors and uncertainties need to be quantified.

Extensive efforts have been put towards the development of precipitation gauge corrections to correct for wind-induced undercatchment errors of snow. From 1986 to 1993, the World Meteorological Organization (WMO) conducted a gauge intercomparison study that took place in 13 countries at 26 test sites and focused on the measurements of frozen hydrometeors (WMO Solid Precipitation Measurement Intercomparison; Goodison et al., 1998). Correction procedures were then derived from the comparison results to correct for systematic errors in precipitation measurements (Sevruk et al., 2009). For instance, the WMO intercomparison results were used to develop a precipitation adjustment function for wind-induced errors on the U.S. National Weather Service (NWS) 8-inch standard *manual* gauge (Yang et al., 1998b). To address wind-induced errors associated with *automatically* recording gauges, the WMO – Solid Precipitation Intercomparison Experiment (WMO – SPICE) began in 2010. Both of the WMO intercomparison studies used the DFIR wind shield design to produce a gauge-based precipitation reference for which unshielded or poorly shielded gauges were compared to. From three years of winter data (snow only) at the Hauleliseter test site in Norway, a continuous adjustment function, with estimated uncertainty and valid for wind

speeds up to 20 m/s, was developed with a Bayesian model selection process (Wolff et al., 2015). The correction model presented by Wolff et al., 2015 is the only method we are aware of that attempted to estimate uncertainty from joint probably distributions of model parameters. Rigorous testing of catch efficiency (CE, DFIR/poorly shielded) transfer functions performed in Kochendorfer et al. 2018 suggests that the derived exponential decay function in (Kochendorfer et al., 2017b), that includes air temperature, gauge height wind speed, and three fitted coefficients, is the best available correction for solid and mixed precipitation measurements from unshielded weighing gauges across a variety of sites.

Despite the fact that quantifying uncertainty in meteorological records is just as important as the accuracy of the records, few methods have focused on gauge-based precipitation uncertainty estimation. Most of the research on precipitation measurement uncertainty is focused on remote sensing (ground and satellite radar; Michaelides et al., 2009; Peleg et al., 2013), regional downscaling and reanalysis of climate models (Cane et al., 2013; Dai, 2006; Langousis et al., 2018), distributed hydrological models (Herrnegger et al., 2018; Westrick et al., 2002; Winstral et al., 2013), or spatial interpolation between gauges (Daly et al., 2017; Diodato, 2005; Frei and Scha, 1998; Lundquist et al., 2015; Sun et al., 2018). Nevertheless, there is also ample opportunity to better understand gauge uncertainties. Gauge correction models and transfer functions provide a means to estimating uncertainties associated with gauges by empirically and/or statistically describing the inherent errors in measurements. However, most gauge correction methods thus far only allow for a single uncertainty term to be applied at each time step

in the record. For instance, despite demonstrating an increase in the error variation with increases in wind speed, Kochendorfer et al. 2017 only report a single uncertainty estimate for every 30-minute accumulation in their snow and mixed precipitation catch efficiency (defined as the ratio of reference gauge accumulation to non-reference gauge accumulation) transfer functions. Only applying a single uncertainty term is not appropriate when variation in the confidence of the correction or accumulation value is dependent on the set of conditions during the time period of observation. For example, we would expect to have lower confidence and higher uncertainty under high wind speeds with variable snowflake sizes and higher confidence and lower uncertainty under low wind speeds with dense graupel. Fortunately, applying Bayesian inference (i.e., machine learning) that reallocates credibility to select model coefficients with likelihood information provides a means to understanding the distribution of modeled estimates (posterior distributions) at each time step in the model. In this study, we apply a Bayesian inference approach to estimate daily gauge accumulation uncertainties for a variety of wind speed and hydrometeor conditions during a 1.5-year comparison period at the Niwot Ridge subalpine forest site.

The ability of precipitation particles, especially snow, to fall into a gauge is dependent on the wind regime at the gauge inlet. The under-catchment of precipitation is a product of horizontal winds creating an updraft at the gauge inlet and deflecting particles away from the gauge (Goodison et al., 1998). The turbulence above the gauge can also influence gauge catch (Colli et al., 2016b) and is more of an issue in complex terrain (e.g. forested mountain slopes). Gauge and shield combinations that have the highest collection

efficiency, using a DFIR gauge as standard, also have the greatest reduction in horizontal wind speed from outside the shielding to the gauge orifice (Rasmussen et al., 2011). Airflow modelling employing Reynolds-averaged Navier-Stokes and Large Eddy Simulation models have confirmed this observation by showing the decrease in updraft velocity near a shielded gauge along with demonstrating how hydrometeor trajectories are influenced by turbulent wind behavior above a shielded gauge (Colli et al., 2016a) (Fig. 1-1). It is important to note here that DFIR's performance was determined through comparison with the bush-sheltered Tretyakov gauge in Valdai, Russia that consists of an extensive diameter of dense bushes manicured to gauge height. Given the importance of turbulence, it is plausible that the complex structure of air space within the surrounding bushes is highly efficient at dampening turbulent energy. The double fence design of the DFIR with a Single Alter shield dampens both turbulence and horizontal wind speed to obtain a high catch efficiency (Thériault et al., 2015) (Fig. 1-2).

Figure 1-1: Airflow around the orifice of a standard precipitation gauge as mapped with laminar wind tunnel flow (Rasmussen et al. 2012).

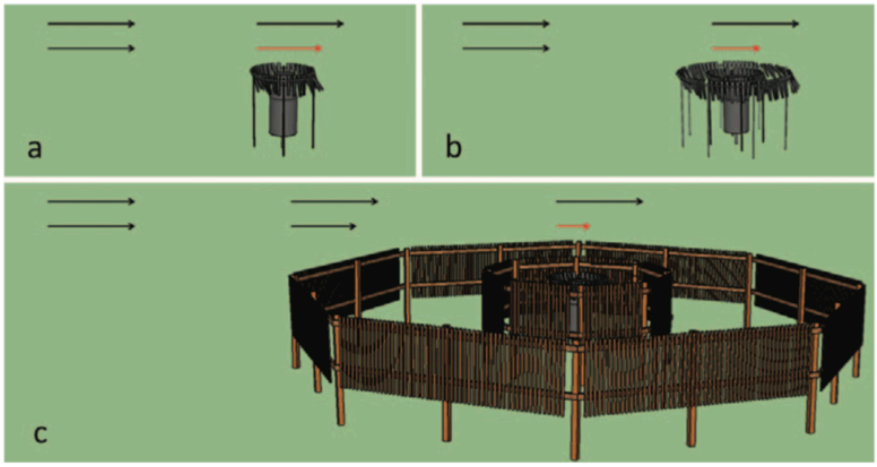

Figure 1-2: Airflow past gauges shielded with a.) single alter b.) double alter and c.) DFIR. The top vectors represent the free-stream air and bottom vectors (orange) represent wind speeds measured at gauge inlet (Rasmussen et al. 2012).

Due to increase drag and smaller gravitational force, snowflakes fall at a slower terminal velocity than rain drops, thus their trajectories are more influenced by updrafts and turbulence near the gauge. Specific temperature and humidity conditions in the atmosphere contribute to cloud ice particle growth (Fig. 1-3) and generate a wide variety of snow hydrometeor crystal types. This variation in crystal size, shape, and density is highly correlated with the collection efficiency of gauges (Thériault et al., 2012) and suggests that gauge under-catch is a combination of wind dynamics and physical parameters of hydrometeors.

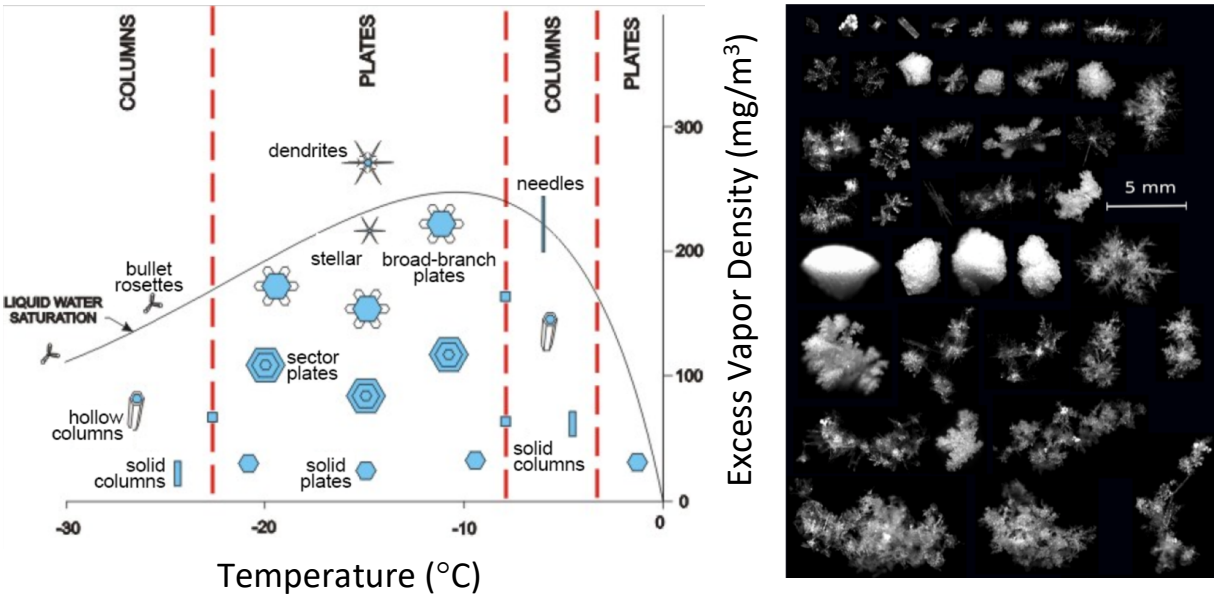

Figure 1-3: Influence of temperature and excess vapor density on snow crystal shapes (plot courtesy of Katja Friedrich). Image on right was taken with the Multi-Angle Snowflake Camera (Garrett et al. 2012) and demonstrates a subset of possible sizes and shapes.

This thesis demonstrates the value of applying a Bayesian machine learning approach to the precipitation gauge correction problem. We show that our gauge correction is not only an improvement over current methods, but is unique in providing reasonable gauge uncertainty estimates. We also show that information on hydrometeor diameter and fall velocities did not significantly improve gauge corrections, but provided more explanatory power than wind speed information and corroborates current understanding of particle flow around a gauge orifice. We develop this Bayesian gauge correction model using precipitation data from a subalpine forest gauge, contributing to a 66-year-long record, that contains large errors in part due to inadequate wind-shielding. Our gauge correction model both increases accuracy in, and provides uncertainty estimates for, the

accumulation from an inadequately shielded gauge in a windy mountain environment with complex terrain features.

This thesis is structured as follows: In chapter 2, the subalpine study site is described with a focus on the dynamical mountain winds and the long-term precipitation record at the site. In chapter 2, the instruments and datasets used in this study are described. The Niwot Ridge Cl gauge errors and justification for a correction are presented in chapter 3. Chapter 4 walks the reader through the correction model development and the details of the Bayesian inference method. The gauge correction results and uncertainty estimation are shown in chapter 5 with model statistics comparing a variety of gauge correction approaches. In chapter 6, the results of the study are discussed and the thesis concludes in chapter 7 with implications that our novel gauge correction and uncertainty estimation has on understanding the role of mountain precipitation in a variable and changing climate.

Chapter 2

Study Site, Datasets, and Instruments

2.1 Study Site

The precipitation gauges and meteorological instruments used in this study were located in a subalpine forest at an elevation of 3030 m above sea level (40°02'11"N 105°32'32"W) on a ~ 5% east-facing slope near Niwot Ridge, Colorado (Fig. 2-1). This site, known as "C1", was established in 1952 by the Institute of Arctic and Alpine Research (INSTAAR) and the Mountain Research Station (MRS) of the University of Colorado, Boulder with initial meteorological measurements of temperature, precipitation, and wind speed (among others). In 1990 the Niwot Ridge Long Term Ecological Research (LTER, National Science Foundation) site was established and has subsequently provided substantial resources for the maintenance and collection of long-term climate data on Niwot Ridge; an important endeavor where long-term (decadal) trends in air temperature and precipitation are viewed as the primary driving variables of ecological change (Greenland, 1989; Suding et al., 2015). The climatological conditions at C1 are potentially representative of the Colorado Front Range subalpine climate zone with average annual

(1953 – 2014) temperature of 1.7°C and precipitation of 680 +/- 130 mm (+/- 1 standard deviation) (Kittel et al., 2015; MRS and LTER long-term climate records). However, the precipitation record at C1 is questionable given the gauge inter-comparisons conducted in this thesis that compare the long-term precipitation record to newer gauges at the site.

The C1 study site experiences high wind speeds associated with its geographic position 8.3 km east of the Continental Divide (~4,000 m a.s.l.) and 21 km west of the eastern high plains of Colorado (~1650 m a.s.l.). In the winter, winds blow primarily from a west-northwest direction (Fig. 2-2). The mean of the maximum daily wind speed (instantaneous measurement recorded at 5 second intervals; indication of gust strength) for December, January, and February (D-J-F) from the historical record (1966-1982) is 20.3 m/s (Fig. 2-3). Contemporary measurements of wind direction and speed above the forest canopy (located on 26 m tower) further highlight that the strongest winds occur during the winter months (D-J-F) from a west-northwest direction (mean above canopy wind speed of 7.13 m/s (Blanken et al., 2009)) and are often associated with the passage of storm systems. However, wind speeds are dampened near the ground (mean D-J-F windspeed of 4.64 m/s; anemometer approximately 6 m above the ground) due to the natural wind fencing of the forest. Average annual wind speed, from daily averages of wind speed, at C1 between 1990 and 2013 (period with minimal data gaps) was 2.7 m/s.

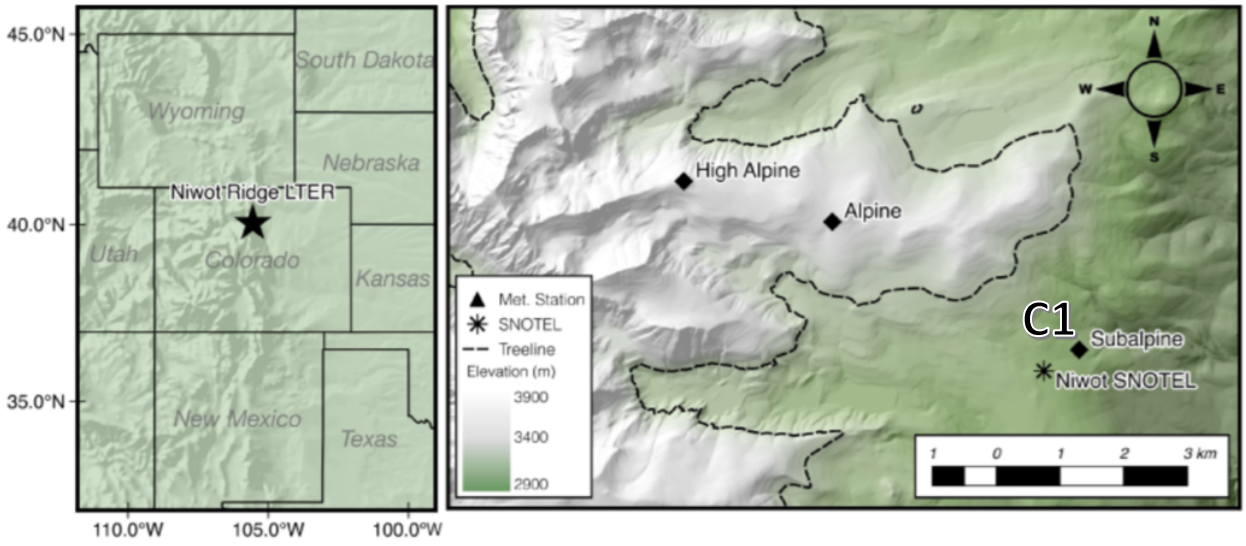

Figure 2-1: Location of the Niwot Ridge LTER and the subalpine ("C1") meteorological station. Map adapted from Jennings et al. 2017.

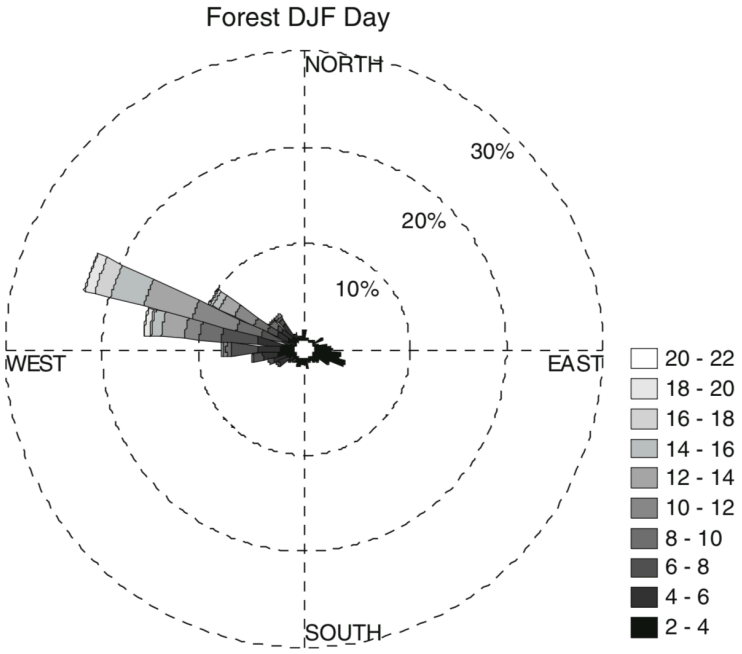

Figure 2-2: Wind rose showing the frequency of 0.5 hour mean wind speed (m/s) and wind direction during the winter months of December, January, and February. Data from a 26-meter tall tower near C1 from December 1, 2007 to February 29, 2008 (Blanken et al. 2009). Only winter months shown due to higher prevalence of flow separation between top of canopy and ground level during the summer months.

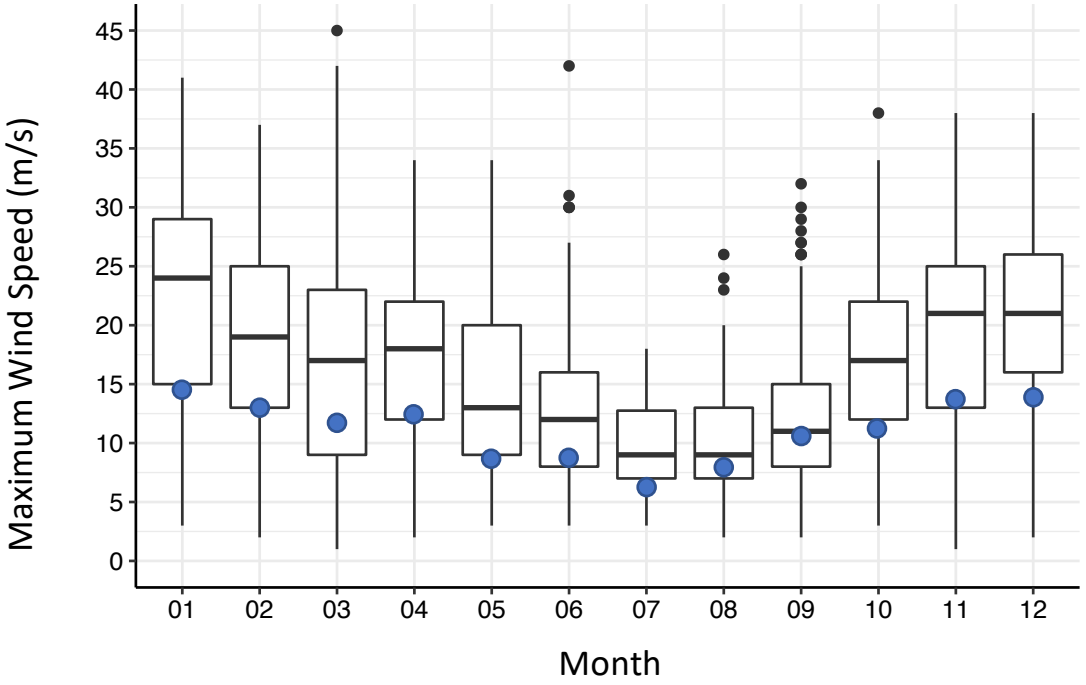

Figure 2-3: Boxplots of instantaneous maximum wind speed for C1 by month. Data are from the 1966-1982 period and from an anemometer ~ 6 meters above the ground recording peak gusts at 5 second intervals. Blue points are monthly averages of the maximum wind speeds recorded during 5-minute periods by the USCRN at ~1.5 meters above the ground during the October 01, 2013 to May, 2015 gauge comparison period used in this study.

The C1 subalpine location experiences cold snowy winters with the average temperature below 0 °Celsius between mid-October through mid-April. Precipitation is common in all months throughout the year (Fig. 2-4) and generally, more than half of the precipitation falls as snow in any given year (Figs. 2-5 and 2-6). Due to the wide range of sub-zero (°Celsius) temperatures, a large variety of frozen hydrometeors sizes and shapes are produced (Fig. 2-7 demonstrates this dynamic during one storm event). Additionally, most snow precipitation events are associated with strong winds (Fig. 2-8) due to greater synoptic scale air pressure gradients in winter. The combination of high winds, significant

snowfall, and variable aerodynamics of hydrometeors potentially drive large errors in the annual liquid water accumulation at the LTER subalpine site.

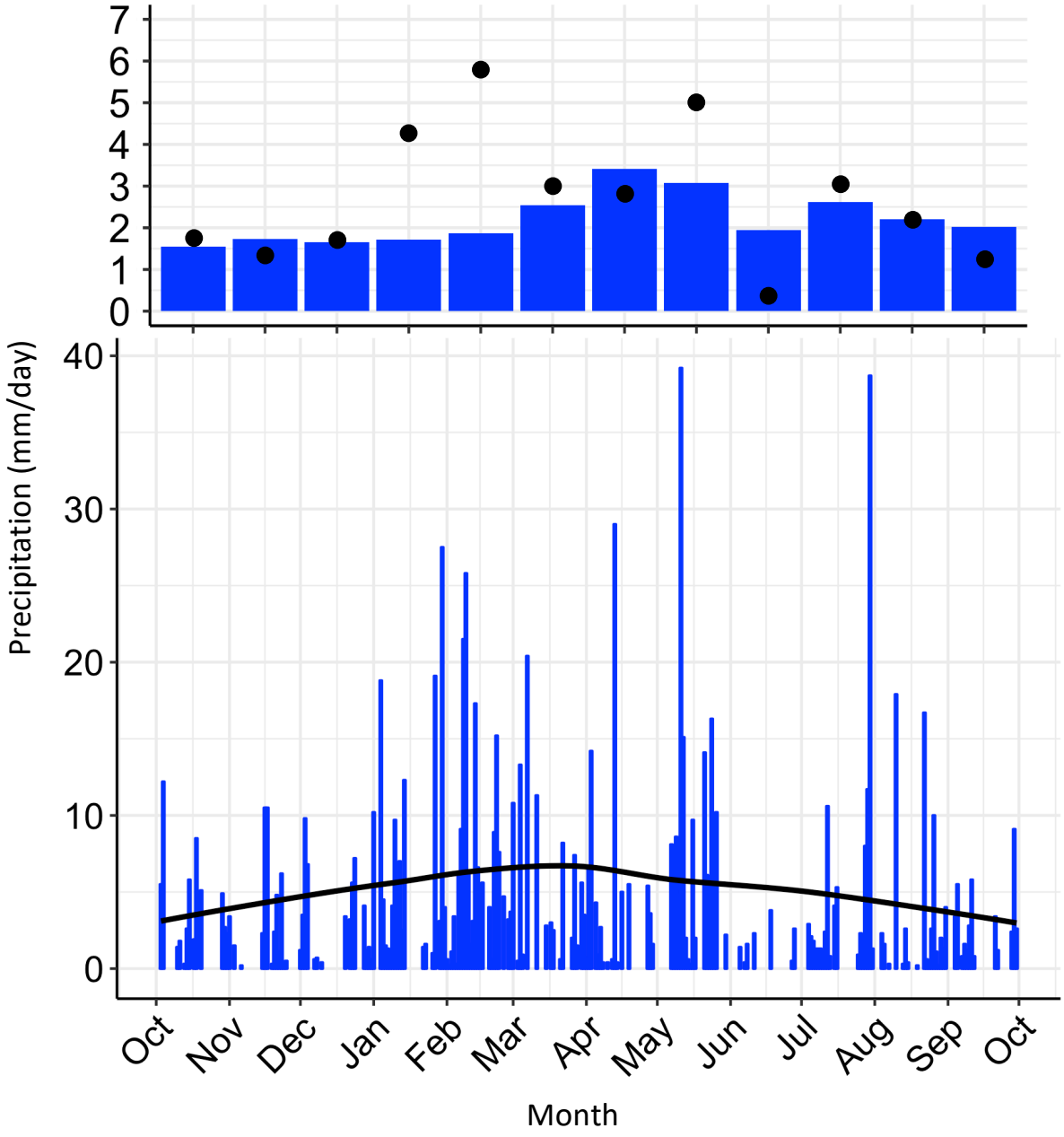

Figure 2-4: C1 Daily precipitation records. a.) The mean monthly precipitation of daily means for the 1953 – 2014 C1 long-term record (LTER-Belfort unshielded gauge) as blue bars and, b.) The daily total precipitation from 5-minute precipitation records for the 2013-2014 water year from U.S. Climate Reference Network gauge near C1. Black line in b. is a local polynomial regression demonstrating the trend in daily precipitation for the 2013-2014 water year. Black points in a. are the mean daily precipitation for each month during the 2013-2014 water year.

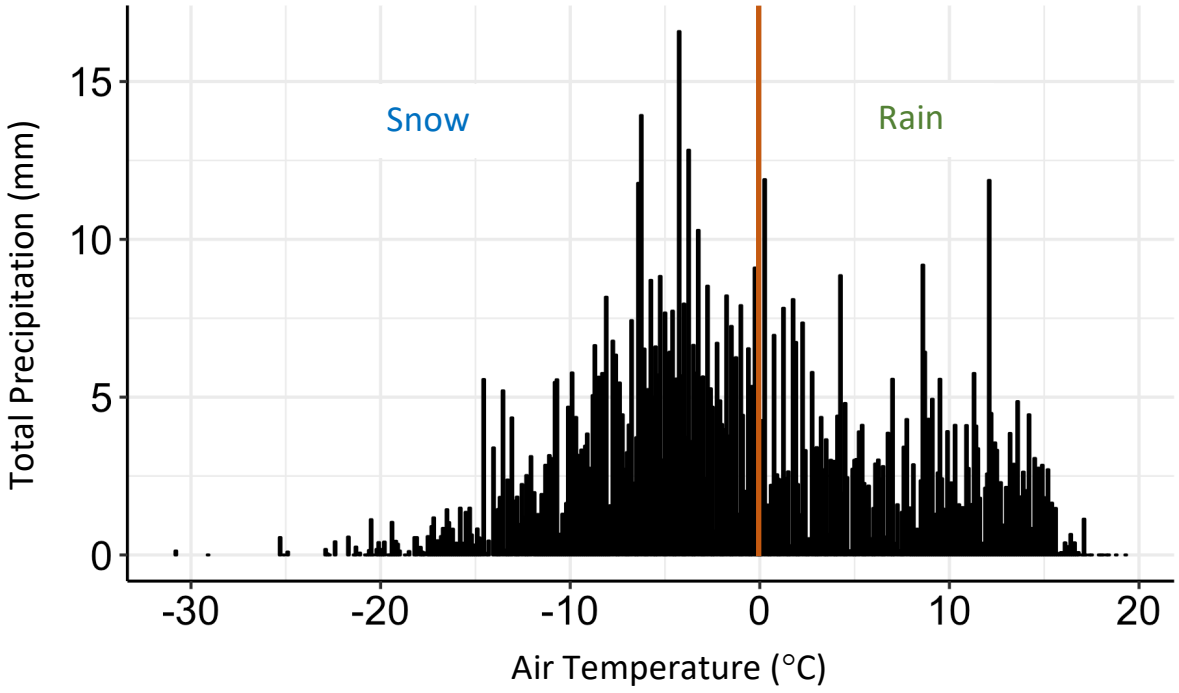

Figure 2-5: Average yearly total precipitation at 0.1 °C temperature bins for the 2004 – 2016 period (total for each bin/12 years) at the C1 site. Precipitation and air temperature data are from the US Climate Reference Network (USCRN) "Boulder 14 W" station located near C1.

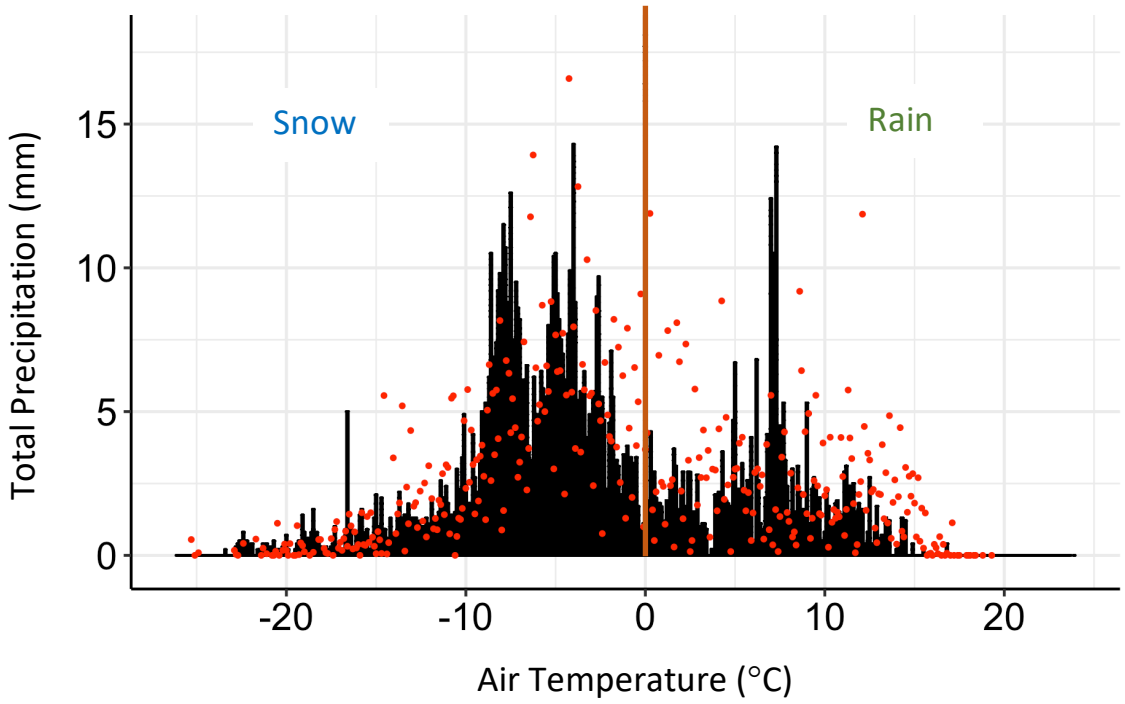

Figure 2-6: Total precipitation at 0.1 °C temperature bins for the 2013-2014 water year at the C1 site. To determine representativeness of the 2013-2014 water year (period used in this study) to the recent decade average, the yearly average total precipitation for the same temperature bins over the 2004 – 2016 period are plotted as red points (data from Fig. 2-5 above). Precipitation and air temperature data are from the US Climate Reference Network (USCRN) "Boulder 14 W" station located near C1.

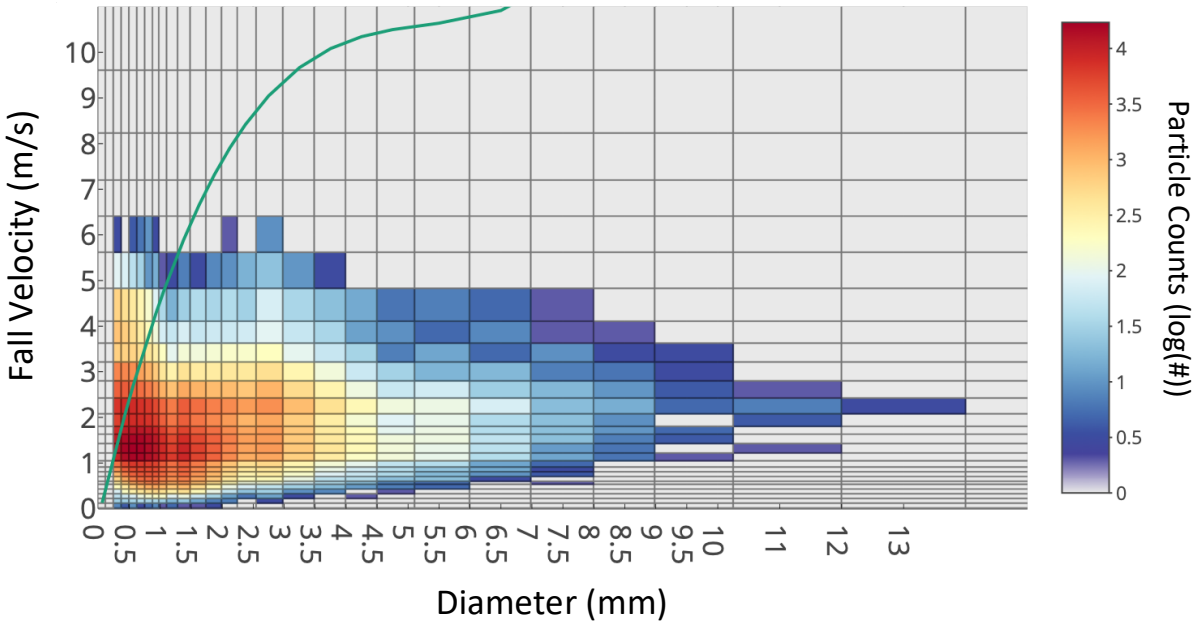

Figure 2-7: Hydrometeor diameter and fall speed distribution for a spring storm (April 16, 2015) where the air temperature started out near -1.5°C and reached -6°C at the end of the event; transitioning from rain, mixed, to snow precipitation types. The green line represents the empirical rain line for diameter and fall speed (Locatelli and Hobbs, 1974); all values on, near, or to the left of this line represent rain and all values to the right of this line represent graupel and snow particles. Data are from laser optical disdrometer at the C1 LTER site.

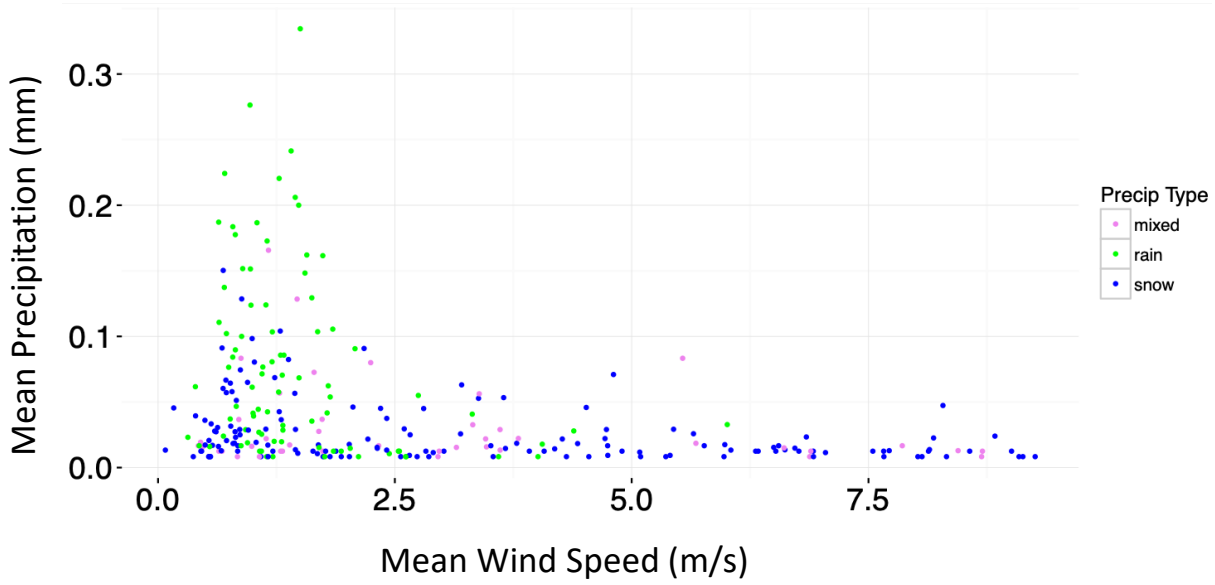

Figure 2-8: Precipitation events for the 2013 calendar year by mean wind speed and mean precipitation. The events are shown by precipitation type: pink = mixed, green = rain, and blue = snow. Precipitation type is classified by applying a +2°C and -2°C cutoff. Events were selected by applying a rolling slope function across precipitation accumulation to find break points; the rate of precipitation for a given time point (5-minute resolution) is determined by considering slope of accumulation 60 minutes before and after that point. For each event, mean precipitation and mean wind speed are calculated. Data are from the US Climate Reference Network (USCRN) station at the site.

In this study, we focus on the October 1, 2013 to May 12, 2013 period to maximize the temporal overlap of the USCRN and LTER-Geonor records with that of the C1-disdrometer. Focusing on this period has allowed us to fully investigate the influence hydrometeor characteristics have on gauge errors. Furthermore, USCRN 5-min records did not begin until 2013 (only daily data between 2003 and 2012) and it was deemed important for the goals of this work to understand how intensity and duration of precipitation events drive gauge errors; information only gleaned from sub-daily precipitation records. Especially when the value of daily uncertainty estimation is considered, this thesis shows that developing a highly skillful gauge correction model on

only 400 days of precipitation, a timeframe that exceeds or closely matches recent gauge correction efforts, is a valid compromise to a less skillful correction model developed on many years of data. Additionally, working with a shorter precipitation period allows for easier detection of gaps and investigation of errors in the record. Given that our gauge correction was developed on a water year (2013-2014) that is representative of the average precipitation, wind, and temperature dynamics at the site (Fig. 2-3, 2-5 and 2-7) there are opportunities to apply the correction results presented here across the entire Niwot Ridge subalpine precipitation record.

2.2 Datasets and Instruments

2.2.1 LTER Long-term precipitation gauges

The LTER C1 site has one of the longest subalpine precipitation records in North America and provides unique insight into the impacts of climate change on mountainous precipitation. Specifically, the climate dynamics of Niwot Ridge, which critically includes C1 precipitation, influences plant community transitions zones (Suding et al., 2015) and impacts the ecosystem fluxes of energy, water, and carbon dioxide across the Niwot mountain catchment zone (Knowles et al., 2015). The position of C1, roughly 900 m below and 8.3 km east of the continental divide, dictates that the C1 precipitation record is regionally relevant to the eastern slopes of the Colorado Front Range but also provides a general understanding of orographic precipitation across the leeward slopes of the Rocky Mountains.

Precipitation data have been recorded at the C1 subalpine site from 1952 to the present. There are however many temporal gaps in the data due to instrument malfunctions or recording errors that have been addressed with gap-filling measures (see Kittel et al., 2015 for details). Given the site-specific nature of wind-induced errors in precipitation measurements, the correction developed in this study focuses on the recent record without any multi-site gap-filling to ensure a properly trained model; ongoing work is seeking to combine corrections and improved gap-filling approaches. Another potential source of error not addressed in this study are instrument and siting changes. From 1952 to 1964 an unshielded U.S. Weather Bureau standard totalizing gauge operated at this site and required manual recordings of accumulation (Fig. 2-8a). In 1961, a Belfort Universal weighing gauge with a potentiometer scale, 324 cm^2 orifice, and chart recorder was installed (Fig. 2-8b). After three years of comparison with the totalizing gauge, the weighing gauge became the operating gauge at C1. Despite the fact that the original Weather Bureau gauge was operated in an opening with little tree cover and the Belfort was installed in a 8-m diameter forest clearing in close proximity, no significant shifts in precipitation patterns were detected (Kittel et al., 2015). In 2000, a Geonor T200B (same as USCRN but without wind shielding) was installed at C1 to compare the Belfort with modern instrumentation (Fig. 2-8c). Our approach here is to focus on improving the accuracy and uncertainty estimation of the C1 precipitation record by using data without gaps from the newer Geonor gauges. Doing so allows us to empirically incorporate local physical conditions (wind, temperature, hydrometeor types) relevant to producing

physically based correction model and avoid confounding effects of comparing different gauge types.

The detection of long-term trends in mountain precipitation is difficult due to large interannual variability in precipitation in mountain regions across the globe (Napoli et al., 2019). This is especially true for the Niwot Ridge C1 long-term (1952-2014) record that has no significant trend in precipitation but very large differences in total precipitation from year to year (Fig. 2-7). The C1 record highlights the need for long-term records to avoid incorrect extrapolation of the record. The lack of a multi-decade precipitation trends have been seen elsewhere across the western U.S.; a dynamic that could be indicative of the influence that individual storms, driven by global atmospheric circulation patterns that change from season to season, have on orographic enhancement of precipitation (Dettinger et al., 2004). Furthermore, recent efforts have been devoted to understanding mountain precipitation patterns in light of the synoptic scale conditions represented in global climate models (Wu et al., 2017). Future predictions of C1 precipitation are thus dependent on a record with accurate measurements at a sub-hourly temporal resolution (historical precipitation recorded daily) that is capable of correlating precipitation accumulation with individual storm characteristics (i.e. pressure gradients and wind speed).

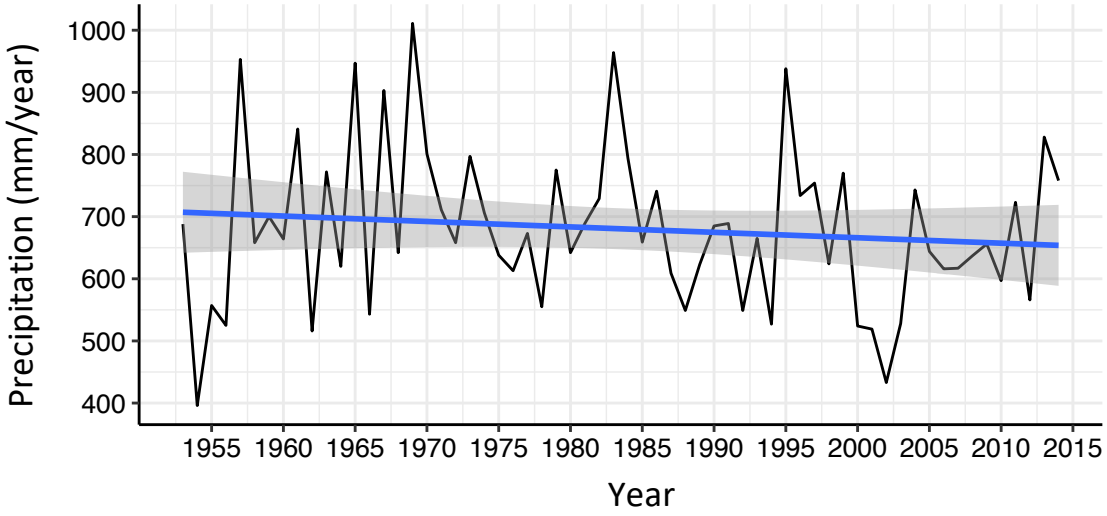

Figure 2-9: The Niwot Ridge C1 precipitation record. Blue line denotes a slight negative linear trend of -0.93 mm/year (P-value: 0.347) and gray shaded area represents the 95% confidence interval in the trend. Data are from the totalizing and Belfort gauges.

a.)

A US Weather Bureau totalizing gauge similar to the gauge used at C1 between 1952 and 1964. Total accumulated precipitation is measured manually at a minimum of once per day (The National Weather Service).

b.)

C1 Belfort Universal weighing-bucket gauge (with chart recorder) in forest opening w/o shield.

c.)

Geonor T200B installed at the C1 site in 2000 and is the gauge used to develop the correction model in this study.

Figure 2-10: Images of the C1 gauges.

2.2.2 USCRN sDFIR gauge

To meet the observational need to measure precipitation at high spatial and temporal resolutions across the United States, the U.S. Climate Reference Network (USCRN) was developed by the National Oceanic and Atmospheric Administration (NOAA). This system of standardized climate observing stations provides long-term observations of precipitation, temperature, and wind speed at 145 stations (some may still be planned) across the US. Fortunately, for the sake of improving past, current, and future records of precipitation for the Niwot Ridge subalpine, a USCRN site was established near C1 in 2003. At C1 and most other locations in the USCRN observation network, precipitation is measured with a Geonor vibrating wire strain gauge with load cells that continuously weigh a collection bucket (Geonor T-200B, 200 cm^2 orifice). The load cell frequencies are converted to collection bucket weight and equivalent depth of liquid precipitation is calculated; a source of error generally not accounted for but potentially important (Katja Friedrich, personal correspondence). A 5-minute average of the depth plus a wetness sensor measurement (presence or absence of precipitation: Vaisala DRD11A Rain Detector) are used to generate 5-minute precipitation amounts (mm/5-min). The weighing gauge is immediately surrounded by a Single Alter wind shield and placed within a small Double Fence Intercomparison Reference shield (sDFIR, two-thirds the diameter of the DFIR; Fig. 2-12). Additionally, the USCRN system consists of a 3-cup anemometer for wind speed and three aspirated/solar shielded air temperature sensors. These additional meteorological sensors are mounted at approximately 1.5 meters above ground surface and represent gauge height conditions. The high temporal resolution of

the USCRN measurements captures the variation in wind speed, temperature, and precipitation intensity within individual storms but more importantly, for the purposes of this thesis, provides measurements that follow international standards, and, therefore, can be used as a basis to correct the poorly-shielded long-term gauges at the Niwot Ridge subalpine site.

Three Aspirated and solar shielded temperature sensors adjacent to sDFIR at C1. Anemometer in the background on boom.

Figure 2-11: USCRN sDFIR near the C1 site. Geonor gauge is in the center and immediately surrounded by the single Alter Shield. The two concentric and hexagonal wind fences are also shown.

The total annual precipitation accumulation from the USCRN sDFIR gauge is significantly more than the LTER-Belfort gauge (one tailed t-test: p-value = 0.0009; Fig. 2-13) and marginally more than the LTER-Geonor (one tailed t-test: p-value = 0.1547; Fig. 2-13). Over the 10-year comparison period (2004-2014), there are large differences in the total accumulated precipitation with both the LTER-Geonor and LTER-Belfort undercatching the amount recorded by the USCRN. Given that the sDFIR shield is very

close to the DFIR WMO standard in performance (Rasmussen et al., 2011) and was selected by NOAA for their standardized CRN network, we confidently assume that the USCRN gauge near C1 provides a quality reference precipitation. The USCRN gauge is 290 meters southeast of C1 in an open area adjacent to the forest and experiences higher wind speeds due to less forest shelter (3.03 vs 2.61 m/s averages for the study period). If the USCRN gauge was unshielded, we would expect more under-catchment from the USCRN due to higher wind speeds at the gauge orifice alone. Although the USCRN is located within a larger clearing than the C1 gauges (60 m vs 8 m diameter clearing), there is dense forest cover immediately to the West and Northwest, primary wind directions at the site, extending to and past C1. With minimal blowing snow at these two locations (anecdotal evidence) there is not much opportunity for over-catchment of precipitation. With a 10-year total under-catch of 1852 mm between the USCRN and LTER Belfort, we claim that the C1 long-term record has systematically and substantially under-caught the true amount of precipitation. However, given that the unshielded Geonor at C1 is not significantly different from the USCRN (mean 10-year under-catch of 60mm) and does not consistently under-catch precipitation, the errors associated with this gauge are more nuanced. For these Niwot Ridge subalpine gauges, it may be combination of wind shielding, difference in the forest clearing geometry, and the particulars of operation for each instrument that are driving the variation in response to wind and hydrometeor conditions.

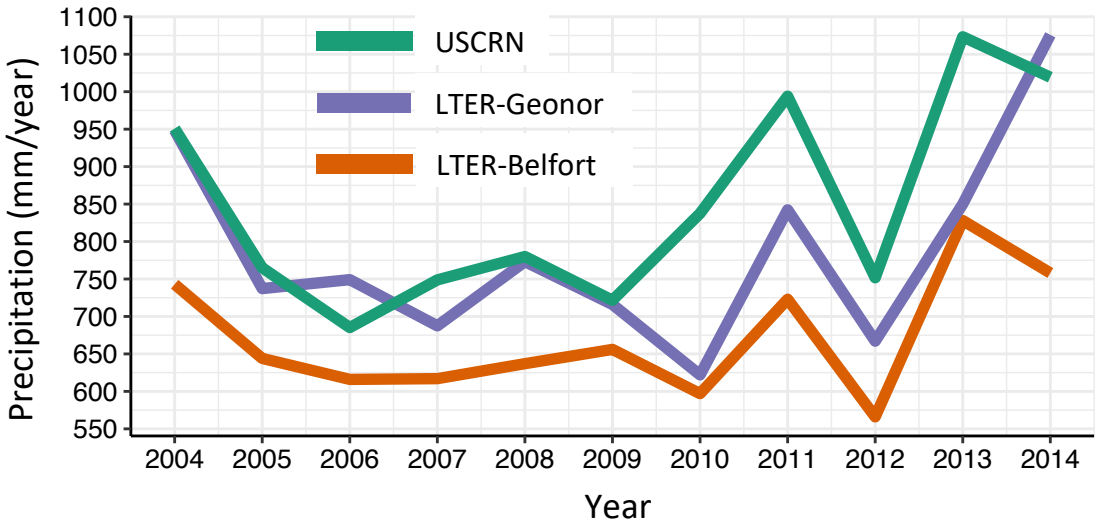

Figure 2-12: Comparison of the USCRN and LTER gauge records between 2004 and 2014. The USCRN record is in green, LTER-Geonor record is in purple, and the LTER-Belfort record is in orange. The 10-year mean precipitation for the USCRN gauge is 848 mm, LTER-Geonor is 788 mm, the LTER-Belfort is 671 mm.

2.2.3 Disdrometer

Detailed hydrometeor parameters are observed with a laser based optical disdrometer that is capable of distinguishing hydrometeor sizes and fall velocities. Disdrometers have proved to be valuable instruments for validating radar-derived rainfall rates and observing microphysical conditions throughout a variety of storm types (Friedrich et al., 2013). Since fall speed and size/shape determine the impact of wind on particle trajectory, disdrometers could also be used to model the spatial distribution of orographic precipitation (windward vs. leeward deposition) (Gerber et al., 2018, 2019; Mott et al., 2014; Woods et al., 2007) and improve mountain weather forecasting. There have recently been efforts to adapt the disdrometer method for ice crystal observations despite the greater challenges associated with the large variety of frozen hydrometeor shapes and

sizes (Battaglia et al., 2010). The wide distribution of size and density in turn creates variable fall velocities and if adequately measured with a disdrometer, hydrometeor information can be used to investigate the role hydrometeor types have on gauge errors. The combination of gauge accumulation, wind observations, and disdrometer based particle size distributions at the C1 site enhance the understanding of how frozen hydrometeors interact with the forest clearings, gauge orifices, and gauge wind shields in the Niwot Ridge subalpine.

The gauge corrections in this study utilize an OTT Particle Size and Velocity (Parsivel) disdrometer operating immediately adjacent to the LTER-Geonor gauge between October 1, 2013 to May 12, 2015. The OTT Parsivel uses a 650-nm laser with a beam area of 54 cm^2 (180 mm long, 30 mm wide, and 1 mm high). As hydrometeors fall through the laser beam their size is estimated with maximum signal attenuation and the speed is estimated by how long the particle remains in the beam (Fig. 2-15). The equivalent snowflake diameter and fall velocity has a larger uncertainty than raindrops since the Parsivel assumes the shape of the hydrometeors to be spheres (Tokay et al., 2014). Other uncertainties arise due to particles falling through the edge of the beam (Battaglia et al., 2010) and due to the deviation of particle trajectories during strong winds (Friedrich et al., 2013).

The Parsivel disdrometer's shortcomings with respect to measuring snowflakes is compensated for with a very high temporal resolution and recording over a thousand size-fall velocity combinations. The raw output of the Parsivel provides a 32 X 32 size versus fall velocity matrix. The observed size ranges between 0.25 and 25 mm and

observed fall speed ranges between 0 and 20 m/s. Precision of the Parsivel decreases with both increasing size and fall velocity and is accounted for through increasing bin sizes; 0.125 to 3.000 mm width for size and 0.100 to 3.200 m/s width for speed. As particles fall through the disdrometer beam they are classified as one of the 1024 size-velocity bins. Over a 10 second interval, the particles detected are summed to provide a total number of particles for the period for each bin. Throughout the duration of a storm lasting approximately one day, the Parsivel disdrometer at Niwot Ridge C1 is capable of measuring over 1 million particles, providing detailed and valuable information on the hydrometeor characteristics.

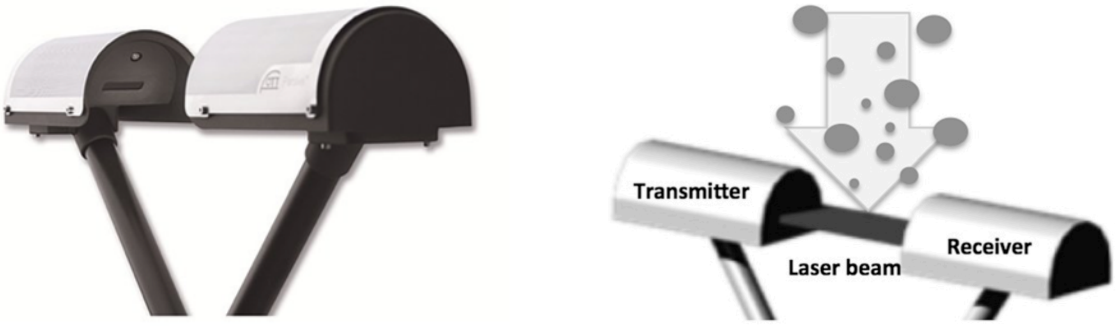

Figure 2-13: Image of the Parsivel disdrometer (a) and diagram of operation (b, Fig. 2 a in Friedrich et al. 2013). The Parsivel consists of a transmitter and a receiver with the laser beam transmitted at a constant voltage throughout operation. Particles falling through the laser beam induce a voltage drop at the receiver that is proportional to the size of the particle and the duration of the voltage drop is proportional to the fall velocity.

All of the instruments described above are relatively close in proximity and represent the subalpine climate zone, however, as previously stated, there are differences in forest cover and clearing size (Fig. 2-14). Furthermore, forest structure at this site has changed considerably over the last century due to fires and logging (Burns; 2018). Therefore, the

airflow patterns, and subsequent influence on hydrometeor trajectories, may be different between the exact locations of the instruments in this study and the differences are likely to have changed over time. We recognize that this is a source of error in our gauge correction efforts but at the same time we argue that our approach is the best way forward to understand and predict the precipitation gauge errors at the Niwot Ridge C1 subalpine site.

Figure 2-14: Satellite image of the LTER C1 subalpine site showing the specific locations of the USCRN, LTER-Geonor, disdrometer, and LTER-Belfort.

Chapter 3

The Niwot Ridge C1 Subalpine Precipitation Gauge Errors

3.1 The difference between gauges at Niwot Ridge C1

There were large differences between the USCRN reference precipitation gauge and LTER-Geonor unshielded gauge (difference = USCRN – (LTER-Geonor)) resulting in different accumulation totals (Fig. 3.1-a) for the 2013-2014 water year that are variable between precipitation type (Fig. 3.1-b). The largest positive differences occurred during the winter months when precipitation type is primarily snow with a mean daily difference of 0.49 mm/day (Fig. 3-2). Rain, with a mean daily difference of -0.42 mm/day, and mixed, with a mean daily difference of -0.23 mm/day, differences are generally smaller than snow but overall are more negative and represent an overall overcatchment of these precipitation types (Fig. 3-2). Interestingly, during the spring months of April – June, there are highly variable differences that are positive or negative. This suggests that the underlying errors are more nuanced during the dynamic spring season and do not lend themselves to simple hypotheses or explanations that have been previously investigated in tightly controlled "test bed" sites. It is for this reason that the approach in this study is

to leverage a machine learning framework capable of detecting unknown errors. However, we still assume that the underlying physical dynamics (i.e., airflow, hydrometeor characteristics, and wind barriers) play a large role in driving the gauge errors.

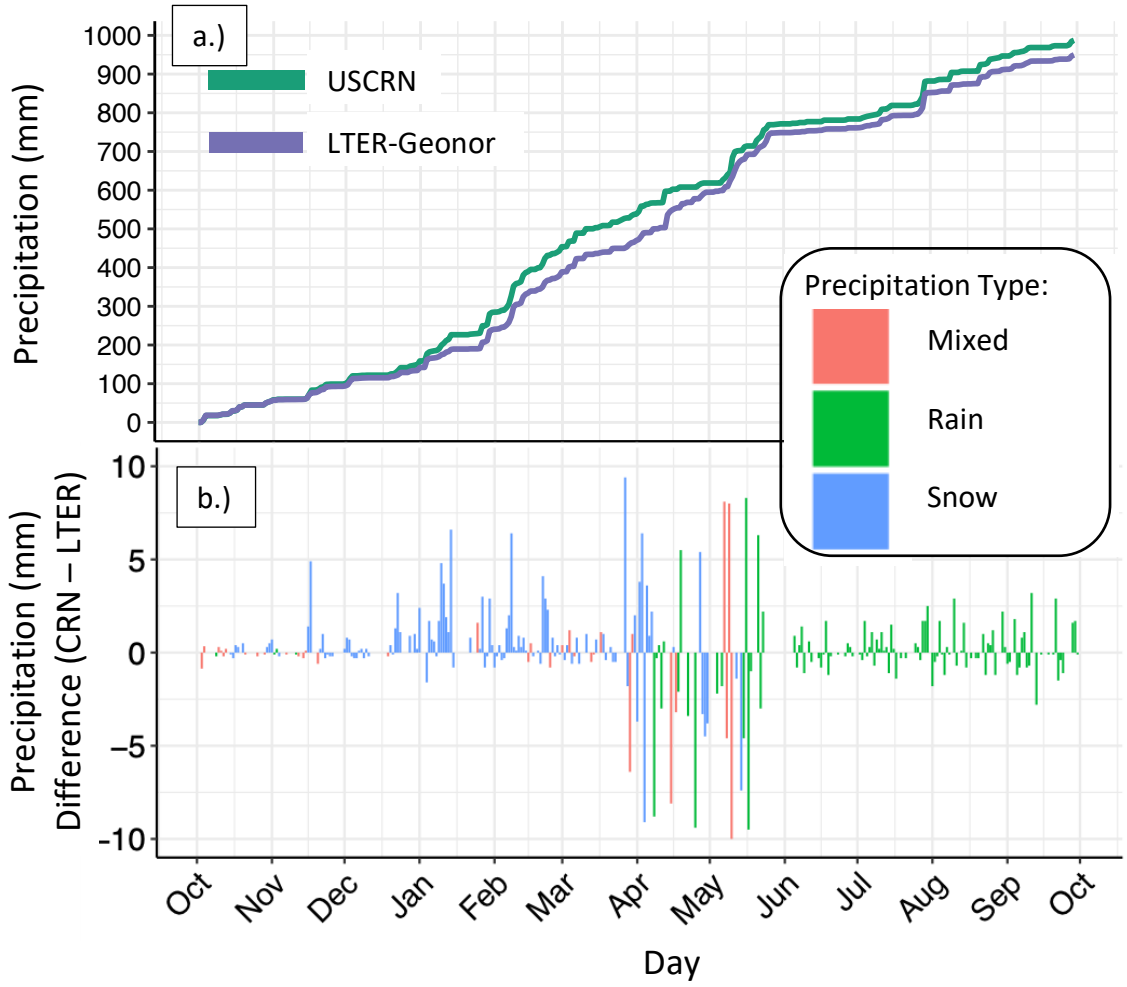

Figure 3-1: Differences in precipitation between the USCRN and the LTER gauges during the 2013-2014 water year. The daily accumulation is shown in (a) with cumulative annual totals of 987 and 950 mm, USCRN and LTER gauges, respectively. Gaps in LTER dataset removed and corresponding USCRN days also removed for comparison accuracy. The daily difference (USCRN – LTER) is shown in (b). All days with gaps in precipitation are removed along with difference greater than 10 mm. The year accumulation is recalculated from non-gap-filled data.

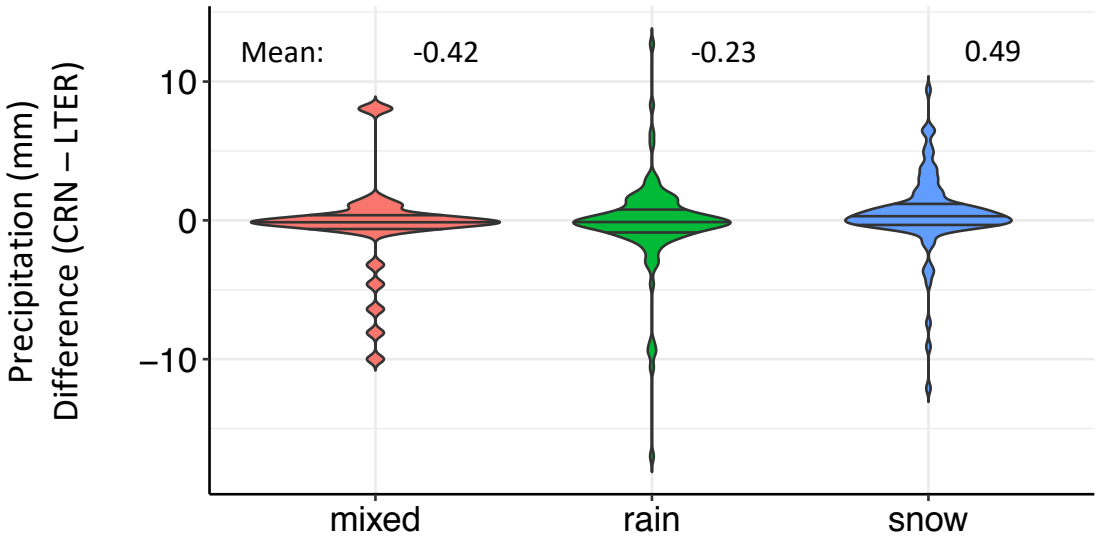

Figure 3-2: Violin plots showing the distribution of the daily total precipitation differences for the 2013 – 2014 water year. Lines within the violins represent the 0.25, 0.50, and 0.75 quartiles. The mean differences (in mm) for the year are displayed at the top of the plot. The overall mean difference across all precipitation types is 0.05 mm/day. Positive values represent under-catch and negative values represent over-catch assuming the sDFIR USCRN gauge is the reference.

3.2 Explanatory variables driving gauge errors

We investigate all of the available and potentially useful information relevant for correcting precipitation accumulation at the Niwot Ridge C1 subalpine. The justification for including wind speed and the hydrometeor characteristics of volume equivalent diameter and number of particles are firmly rooted in published gauge correction methods and approaches previously mentioned. We also investigate precipitation intensity and duration of precipitation to capture systematic errors that are instrument related or interact with physical information. All explanatory variables are split by precipitation type factors following Kochendorfer et al., 2018 by applying +2° and -2° C air temperature thresholds (> +2°C = rain; <= +2°C and >= -2°C = mixed; < -2°C = snow).

3.2.1 Wind Speed

The average wind speed for each day during precipitation periods is obtained from the USCRN 3-cup anemometer located near the USCRN gauge at a height of 1.5 m above the ground. The height of the anemometer is roughly equal to the USCRN gauge orifice and is representative of wind speeds outside of the wind fence at the edge of the forest clearing. To only consider the wind speed during precipitation events, precipitation periods are defined by consecutive 5-minute periods with a 60-minute intensity greater than 0 mm/hour. This is calculated automatically in the R programming language by invoking the “run length encoding” (rle) command and then averaging the wind speed during the defined precipitating period for a given day.

There is large scatter in the mean wind speed as a function of the gauge precipitation difference but there is detectable variation in the trend between precipitation types (Fig. 3-3,a). The increasing difference trend between the two gauges for snow is what we would expect if the poorly shielded gauge is under-catching snow and is in line with previous observations and modelling of lower catch efficiency at higher wind speeds for frozen hydrometeors (Thériault et al., 2012). Both the mixed and rain precipitation types have a negative trend in gauge difference for increasing wind speeds.

3.2.2 Precipitation Intensity

Precipitation intensity is estimated from the 5-min USCRN precipitation totals. The 15-minute intensity (i.e., rate of precipitation) for a given time point (5-minute resolution) is calculated by taking the slope of accumulation 5 minutes before and after that point; this is achieved in the R programing language by calling the "rollapply" function on a "zoo" time object. This value is then multiplied by 4 to obtain the mm/hour units. We use the daily maximum 15-minute precipitation intensity by taking the maximum value for each day.

Figure 3-3,b shows that there is a strong positive difference in precipitation (USCRN > LTER) for increasing intensity with snow showing the strongest effect. The points at 0 mm/hour max intensity correspond to cases when the USCRN did not measure precipitation for the day but the LTER gauge did.

3.2.3 Precipitation Duration

The duration of precipitation in a given day is calculated by first defining precipitation events and then summing the duration of those events. Events are defined in the same way described for mean wind speed. This inevitably calculates durations that are longer than the actual time of precipitation but the method is consistent and a reasonable approximation.

The strong positive and linear increase in gauge difference for increasing duration suggests that there are systematic errors that accumulate linearly over the course of a precipitation event (Fig. 3-3,d). The residuals away from the trend line, however, indicate that more than a simple adjustment is required to correct the LTER gauge.

3.2.4 Volume Equivalent Diameter

The volume equivalent diameter (VED, the diameter of a particle assumed to be a sphere), was derived from the C1 Parsivel disdrometer. To calculate the daily average VED from the raw Parsivel data the following steps were taken: 1.) number of particles in each diameter class were counted for each day, 2.) counts were multiplied by their respective size class median value, 3.) values generated in step 2 were summed then divided by the total number of particles for that day to produce an average diameter value. The hydrometeors were then classified by precipitation type as described above. There was no a relationship between VED and the USCRN – LTER difference for all precipitation types with a large amount of scatter for each diameter class (Fig. 2-3,e). This suggests that knowing the average hydrometeor size alone is not sufficient in predicting gauge errors.

3.2.5 Number of Particles

The total number of particles detected for each day is calculated by summing all of the particles in each of the 32 size classes. This value in combination with the fall speed and VED can provide an estimate of liquid equivalent precipitation accumulation. There was a positive relationship between the number of hydrometeors and the USCRN – LTER difference when precipitation is snow but there is no relationship for rain or mixed precipitation (Fig. 3-3,c). Furthermore, there are several days when snow particles total more than one million whereas there is only one mixed and no rain precipitation days above this amount. These patterns indicate that there are greater errors associated with frozen hydrometeors with a higher probability for these errors to occur, compared to rain or mixed events, given the larger amount of snow particles falling at the C1 subalpine site. These observations imply that snow hydrometeors interacting with the local terrain, forest, and gauge configurations are partly responsible for the observed gauge errors.

There are clear indications that these variables can explain and help to predict gauge errors for the Niwot Ridge subalpine gauges. The variable response between precipitation types highlight the importance of investigating gauge errors for snow, mixed, and rain events separately. With the large scatter (i.e., residuals) around the trend lines, it is also evident that the best gauge correction is likely to include a combination of these explanatory variables in a model capable of prescribing interactions among variables.

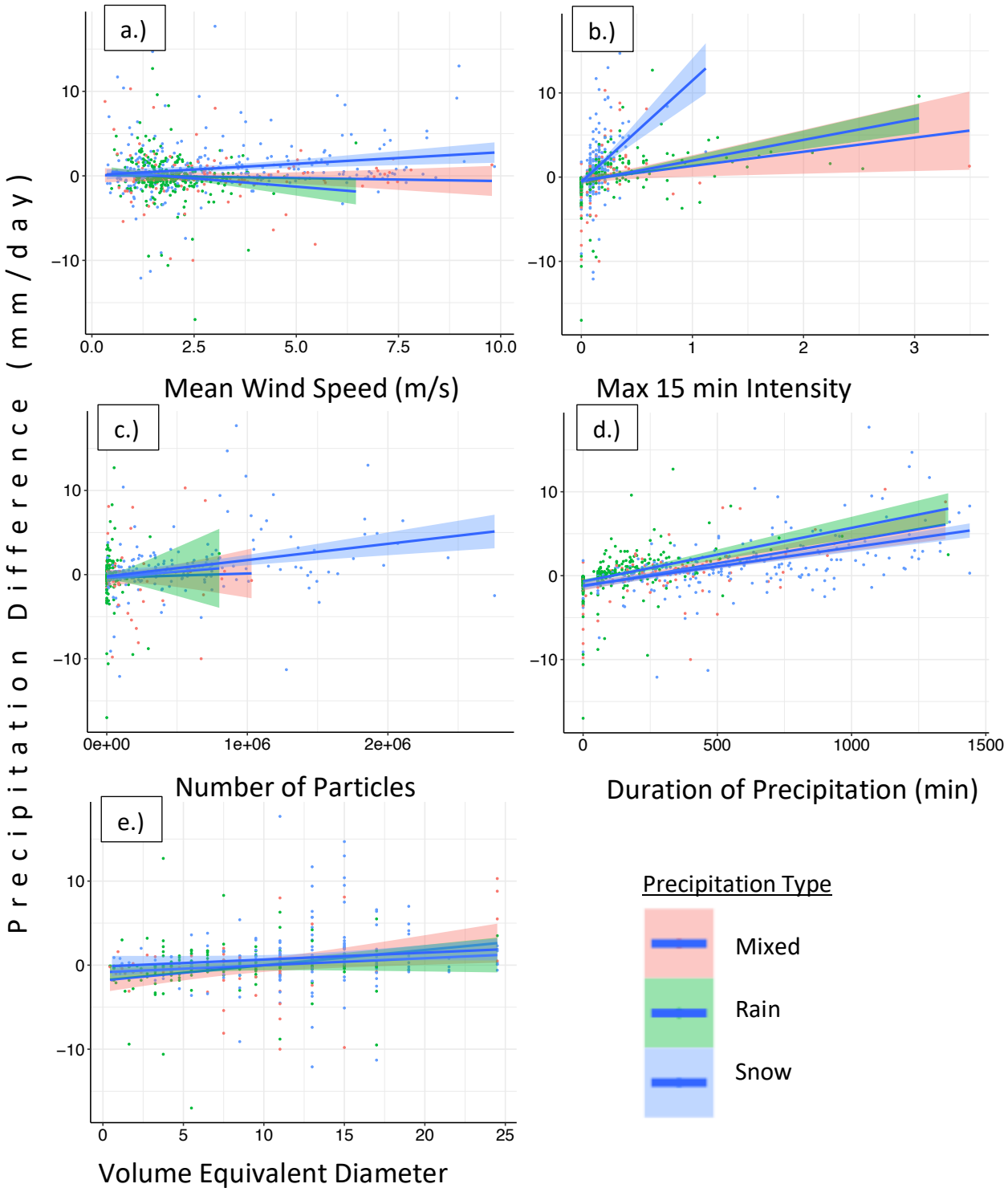

Figure 3-3: Explanatory variables describing the gauge differences. These variables are used in the gauge correction models described in this thesis. Mean wind speed, intensity, and duration are derived from the USCRN station. Number of particles and volume equivalent diameter are calculated from the Parsivel raw output. Shaded regions represent the 95% confidence interval in the trend line.

Chapter 4

The Gauge Correction Model

4.1 Introduction

To address the current uncertainties in precipitation at the Niwot Ridge LTER C1 subalpine site, we develop a hierarchical Bayesian regression gauge correction model (HBayeRGC) to explain the difference in precipitation accumulation between the U.S. Climate Reference Network small Double Fence Intercomparison Reference gauge (USCRN sDFIR) and the LTER long-term Geonor gauge. We accomplish this task by first selecting the best linear regression model from the available explanatory variables (i.e. covariates). Once we have a reasonable linear regression model that considers interactions between all variables, we calculate the probability distribution functions (PDFs) for each explanatory variable and the dependent gauge difference response variable. These PDFs are then sampled within a Bayesian model framework as *likelihood* information to fit the same best linear regression model. Furthermore, the Bayesian model is formulated to incorporate *prior* knowledge of the linear model coefficients to

provide reasonable starting points for the iterative and machine learning process of determining the *posterior distribution* of each Bayesian model coefficient and the predicted response. This approach allows for a gauge correction model that has higher predictive skill and can estimate uncertainty for each set of explanatory conditions or in the case here, for each day in the precipitation record.

The correction models in this study use data from October 1, 2013 to May 12, 2015, dictated by the limited disdrometer record at C1. All gaps were removed from the datasets and only overlapping days from the USCRN gauge, LTER-Geonor gauge, and disdrometer are used. Gauge differences (USCRN minus LTER-Geonor) are predicted at the daily time scale due to the daily time resolution of the LTER-Geonor gauge. All data management and statistical programing is performed in the R computing language.

4.2 Multiple Linear Regression Model

To determine the best combination of explanatory variables, and the interactions between them, that best explain the gauge difference and provides the Bayesian model with an objective linear regression framework, a multiple linear regression (MLR) model was fit to the data. The MLR model was developed from the standardized (mean = 0, standard deviation = 1) response and scaled (standard deviation = 1) explanatory variables described above; wind speed, precipitation intensity and duration, number of particles, and volume equivalent diameter (VED). Insight on possible variable interactions are gleaned from Figure 4-1. To pick the most parsimonious model that minimizes the residual sum of squares the Akaike Information Criterion (AIC) was used:

$$AIC = -2 * \ln(L) + 2 * K \qquad \text{Equation 1}$$

where L is the maximum value of the likelihood, and k is the number of estimated parameters. The maximum likelihood for AIC is the joint probability distribution of the random sample evaluated for the set of observations. The AIC is used in a forward and backward model selection that considers all combination of variables and interactions. The best model is then compared to the simplest model to ensure statistical significance and a reasonable increase in variation explained. The formulation of the best linear regression gauge correction model is:

Equation 2

USCRN - LTER ~ Precipitation Type + Total Particles + Mean 15-minute Intensity +
Mean Volume Equivalent Diameter + Duration + Mean Wind Speed +
Precipitation Type * Total Particles +
Mean Volume Equivalent Diameter * Total Particles +
Mean 15-minute Intensity * Total Particles

where * denotes an interaction and precipitation type is a regression factor. The MLR has an adjusted R-squared (adj R^2; adjusted for number of predictors in the model; measure of variance explained) of 0.461 as compared to an adj R^2 of 0.023 for a simple model with only precipitation type and wind speed. All coefficients, including interactions, are statistically significant (Table 4-1). The predicted values are recovered by multiplying the standardized predicted value by 3.33 (scale) and then adding 0.25 (center).

Table 4-1: Coefficients table for the multiple linear regression predicting the USCRN – LTER gauge difference. Residual standard error is 0.7342 on 388 degrees of freedom. The adjusted R-squared is 0.461 and model p-value is < 2.2e-16. Coefficient significance codes: 0 '***' 0.001 '**' 0.01 '*'

Coefficient	**Estimate**	**Std. Error**	**t-statistic**	**P-value**
Intercept	-0.59449	0.08942	-6.648	1.01e-10 ***
Mixed	0.32046	0.10257	3.124	0.001915 **
Rain	-0.89671	0.16166	-5.547	5.39e-08 ***
Snow	0.57625	----------	----------	----------
Total Particles	-1.50178	0.16775	-8.953	< 2e-16 ***
Intensity	0.77643	0.08541	9.091	< 2e-16 ***
VED	-0.33292	0.06114	-5.445	9.22e-08 ***
Duration	0.35491	0.08253	4.300	2.16e-05 ***
Wind Speed	0.12021	0.05125	2.346	0.019486 *
Mixed*Particles	0.52719	0.16612	3.173	0.001626 **
Rain*Particles	-1.59506	0.26064	-6.120	2.29e-09 ***
Snow*Particles	1.06787	----------	----------	----------
VED*Particles	-0.46693	0.08260	-5.653	3.07e-08 ***
Intensity*Particles	-0.09140	0.02686	-3.402	0.000738 ***

With a multi-dimension linear regression gauge correction model that includes three interaction terms, it is difficult to explain the direct effect of any one explanatory variable. However, we can say with confidence that all variables, including the precipitation type, are important in explaining the gauge differences in the presence of all other variables and interactions in the model. The "total particles*intensity" and "total particles*VED" interaction terms are climatologically relevant given the varying relationship among these variables by precipitation type; for example, days with more hydrometeors recorded tend to be snow events with higher precipitation intensity and larger particle sizes (Fig. 4-1,b,c). The relationship between duration and intensity highlights the fact that winter storms are longer in duration with summer convective storms being shorter in duration (Fig. 4-1,a). There are relatively low correlations (R) between all variables (Fig. 4-2) confirming the usefulness of including each variable. The exceptions to low correlation are between duration – intensity and duration – total particles, hence why the "duration*intensity" interaction is not used, but all of these variables are highly significant in the model (p-value < 2.16e-05). The p-values (probability there is no effect) offer insight on the relative importance of each coefficient (explanatory variable) in the model. Therefore, it is interesting to see that wind speed has the highest p-value. Although wind speed significantly helps to explain the gauge differences at C1 and corroborates current understanding of wind-induced gauge errors, there is a lot more addition information capable of explaining the errors at the Niwot Ridge subalpine site.

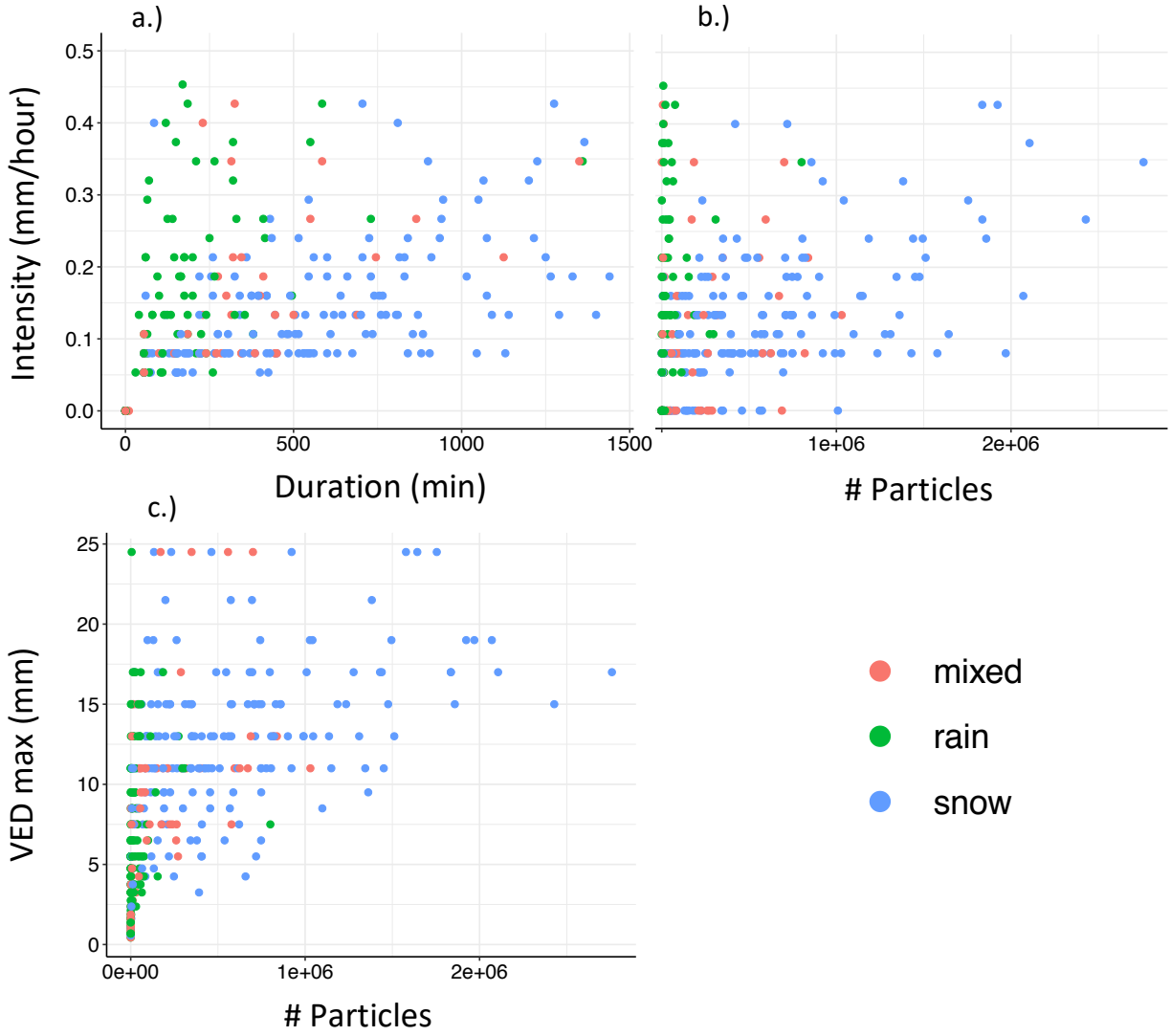

Figure 4-1: Scatter plots of the relationship between duration and intensity (a), number of particles and intensity (b), and number of particles and maximum volume equivalent diameter (c) for the October 1, 2013 to May 12, 2015 gauge comparison period.

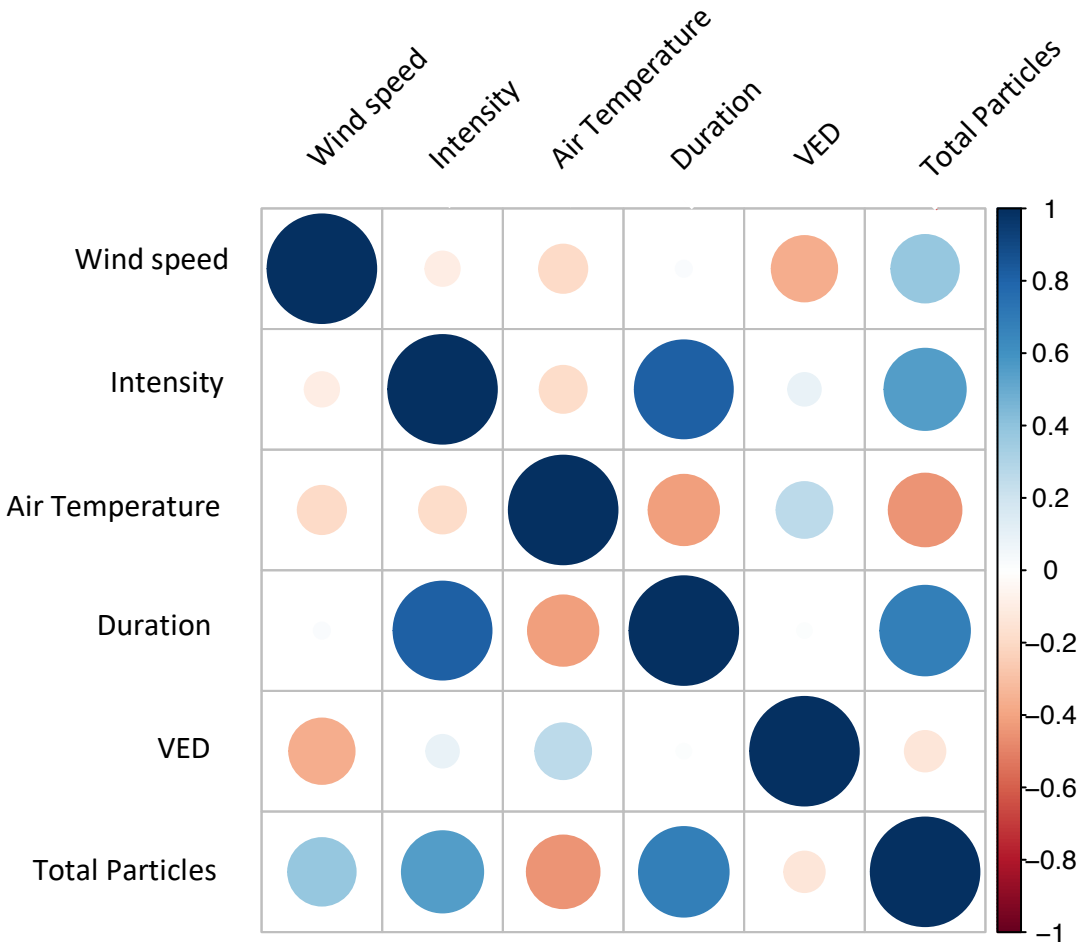

Figure 4-2: Correlation between all explanatory variables of interest. The size of the circle is proportional to the absolute value of the correlation and the color represents either positive (blue) or negative (red) correlation.

4.3 Hierarchical Bayesian Regression Gauge Correction Model (HBayeRGC)

Gauge and disdrometer measurements of precipitation are error prone. This is especially true in complex mountain terrain where there are potentially many sources of errors and is the motivation in this thesis for uncertainty estimation. The probability distributions (PDFs) of the meteorological data are unique to each variable and can be generally describe as gamma distributions. Therefore, recorded precipitation values, along with other sources of meteorological data, should be described in terms of likelihood and probabilities rather than absolutes. To more accurately model gauge errors without violating regression modeling assumptions on PDFs, as was done with the MLR, a modelling framework that allows for the specification of unique PDFs is required. Furthermore, information contained within the structure of the data, which approximate the true distribution of potential observations, can be used as additional model structure in a machine learning approach, with demonstrated improvements in model predictive skill for meteorological data (Rasouli et al., 2012). This is the inspiration and justification for the use of Bayesian statistics in precipitation gauge corrections.

Bayesian statistics allows for linear regression models to be parameterized from response and explanatory probability distributions. In the case of the linear regression gauge correction model described in the previous section, we can assign a probability of obtaining any given value within the range of precipitation differences and explanatory values used in the model. These probabilities of model variables, as determined from C1 observational datasets, provide distribution parameters (e.g., shape, scale, and location) used within the Bayesian model (Fig. 4-3). Given our prior knowledge of the importance

of precipitation type and to strive for model simplicity, the gauge correction dataset was split into mixed, rain, and snow to create a Bayesian correction model for each type is described below in section 4.3.2, 4.3.3. and 4.3.4 (equations 3-5). Additionally, the prior knowledge of model coefficients was used to define starting values for the Bayesian model selection. The Bayesian process employed here uses a random walk approach (Markov Chain Monte Carlo) that samples from the probability distributions shown in Figure 4-3 (approximations of the true values) to re-allocate credibility and produce posterior distributions that result in the most likely model solution. All standardized explanatory variables (scaled to 1 standard deviation, no centering) are approximated with the Gamma distribution with shape ($mean^2/sd^2$) and scale ($sd^2/mean$) parameters defined in Tables 4-2, 4-3, and 4-4. The distributions of the observed gauge differences were determined to approximate the Cauchy distribution with a location of 0 and scale of 1 and defined within the HBayeRGC as a Student's *t* distribution with 1 degree of freedom.

For each of the mixed, rain, and snow HBayeRGCs we use five chains (stochastic sampling of PDFs with varying starting points) and 15,000 iterations with a burn-in of 500 and thinning of 50. The Bayesian hierarchical model samples from the PDFs described here with Markov Chain Monte Carlo (MCMC) simulation is performed with the Just Another Gibbs Sampler (JAGS) program. The complete formulation of each HBayeRGC with priors and likelihood information for each model variable is shown in Appendix A. The posterior coefficients and model diagnostics are displayed in Tables 4-5, 4-6, and 4-7 with plots of posterior distributions of the coefficients in Figures 4-4, 4-5, and 4-6. For additional information on Bayesian theory, JAGS programing, and the

implementation of these models in R, see John K. Kruschke's book: Doing Bayesian data analysis: a tutorial with R, JAGS, and Stan (2nd edition, 2014).

4.3.1 Data management and analysis workflow

The implementation of a Bayesian gauge correction model is more than applying a simple correction equation or transfer function. The novelty and success of such an approach lies in the incorporation of prior knowledge of physical relationships, modelling with best estimates of probability distributions, and understanding the outcome in terms of likelihood information. Here are the simplified steps taken and proposed in this thesis to achieve a Bayesian gauge correction model (see appendix A for full Bayesian model formulation):

1. Combine gauge data w/o gaps and calculate difference in daily accumulation.
2. Merge wind speed, disdrometer, and sub-hourly precipitation statistics and scale data.
3. Select a best linear regression model (MLR) with all potentially useful information to form preliminary understanding of physical drivers of the gauge errors (equation 1).
    a. Use as simple correction for new gauge data by inserting new explanatory data into equation 1.
    b. Add the predicted difference value to unshielded gauge daily accumulation
    c. Use HBayeRGC posterior distributions of model coefficients to apply uncertainty.
4. If precipitation type a significant model factor, select additional best MLRs for rain, mixed, and snow precipitation type.

a. Split data and re-run MLR selection.

b. Repeat steps 3a-c as alternative to running full HBayeRGC.

5. Determine the PDFs of scaled gauge differences and explanatory variables (Fig. 4-3 and tables 4-2, 4-3, and 4-4).
6. Formulate Bayesian model with prior knowledge of regression coefficients (e.g. Table 1) and the model variable PDFs as likelihood information.
7. Employ Gibbs sampling to run MCMC algorithm and generate posterior probabilities of the predicted gauge differences and explanatory coefficients.
8. Correct unshielded or non-reference gauge with predicted gauge differences.
9. Predict gauge errors for gauges without a nearby reference but with similar explanatory information by adding new explanatory information as inputs in the HBayeRGC and re-running the model to obtain new estimates.
    a. Use same linear regression models (equations 3, 4, and 5) and Bayesian model coefficients (tables 5, 6, and 7).
    b. Assumes same gauge difference and explanatory PDFs.
    c. Or simulate new PDFs if new site characteristics dictate the use of alternative linear regression models.
        i. Formulate a site-specific HBayeRGC.
10. Use posterior distributions of predicted and explanatory estimates to apply daily uncertainty information to gauge records.

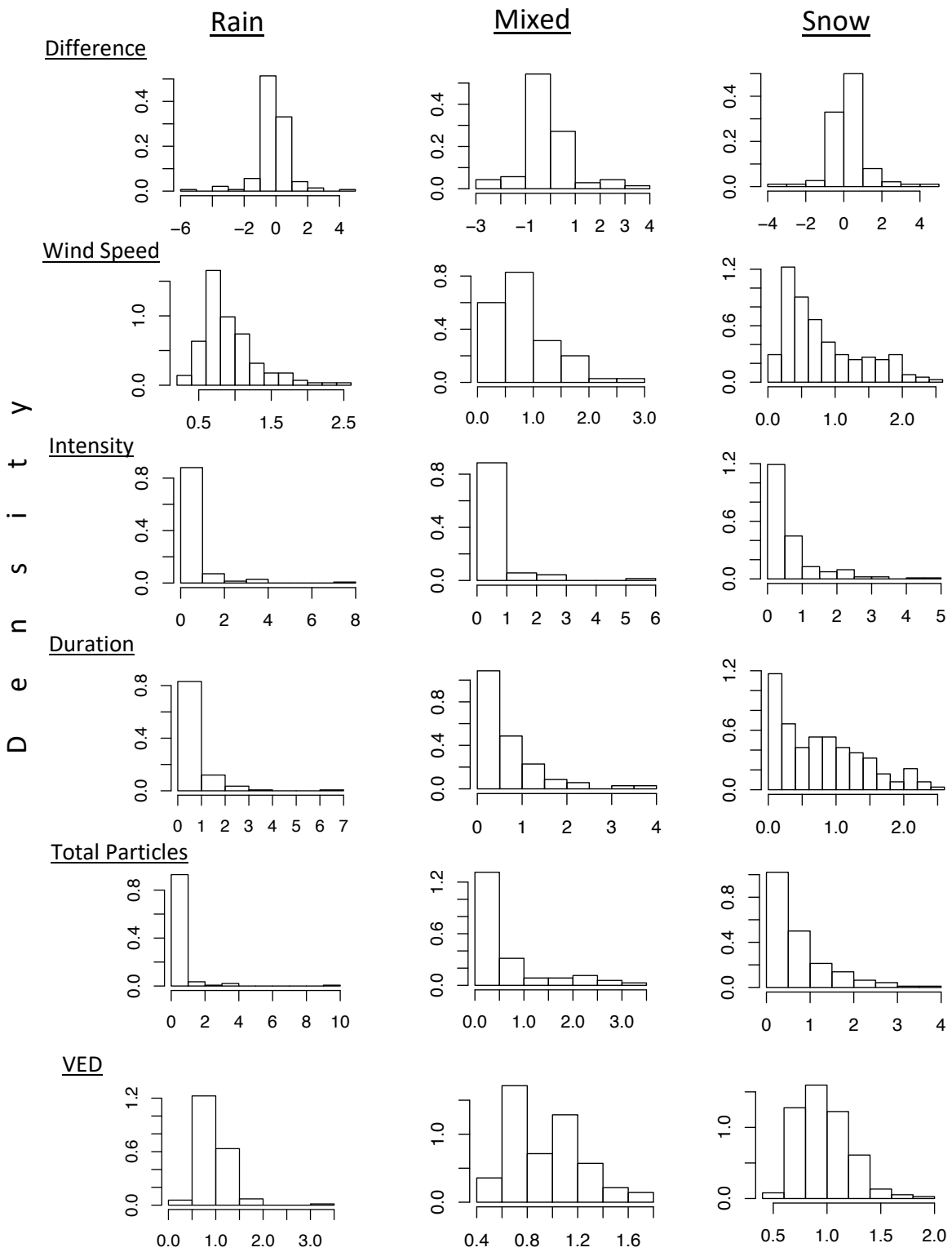

Figure 4-3: Density distribution plots for each scaled correction model variable. These plots visualize the probability distribution functions (PDF) for which the PDF family and parameters are estimated from. All explanatory variables are described as gamma distributions. A Cauchy distribution is used for the difference.

Table 4-2: Gamma distribution parameters for the rain precipitation type HBayeRGC Model

Parameter	Shape	Scale
Wind speed	5.738079	0.1603397
Intensity	0.2165204	1.947229
Duration	0.4173668	1.298814
Total Particles	0.1362195	2.540766
VED	7.738119	0.121231

Table 4-3: Gamma distribution parameters for the mixed precipitation type HBayeRGC Model

Parameter	Shape	Scale
Wind speed	2.580335	0.3272983
Intensity	0.2809226	1.664394
Duration	0.56958348	1.054849
Total Particles	0.4767221	1.189062
VED	10.5412	0.09006869

Table 4-4: Gamma distribution parameters for the snow precipitation type HBayeRGC Model

Parameter	Shape	Scale
Wind speed	1.964305	0.4136813
Intensity	0.6330469	0.9825011
Duration	1.456773	0.5277571
Total Particles	0.9777428	0.7181736
VED	17.4844	0.05548508

4.3.2 Rain HBayeRGC: Linear Regression Component

The rain HBayeRGC model's linear regression component is structured as follows:

```
y.hat[i] <- b0 + b1 * truexr_par[i] + b2 * truexr_int[i] +
    b3 * truexr_dur[i] + b4 * truexr_ws[i] +
    b24 * truexr_int[i] * truexr_ws[i]}}
```

Equation 3

where, b0 = intercept coefficient, b1 = total particles coefficient, b2 = intensity coefficient, b3 = duration coefficient, b4 = wind speed coefficient, b24 = intensity * wind speed interaction coefficient, truexr _ws = sampling of wind speed from gamma distribution, truexr _int = sampling of intensity from gamma distribution, truexr _dur = sampling of duration from gamma distribution, truexr_par = sampling of total particles from gamma distribution, y.hat = the predicted difference (CRN-Met).

4.3.3 Mixed HBayeRGC: Linear Regression Component

The mixed HBayeRGC model's linear regression component is structured as follows:

```
y.hat[i] <- b0 + b1 * truexm_par[i] + b2 * truexm_int[i] +
    b3 * truexm_dur[i] + b4 * truexm_ws[i]}}
```

Equation 4

where, b0 = intercept coefficient, b1 = total particles coefficient, b2 = intensity coefficient, b3 = duration coefficient, b4 = wind speed coefficient, truexm _ws = sampling of wind speed from gamma distribution, truexm _int = sampling of intensity from gamma distribution, truexm _dur = sampling of duration from gamma distribution, truexm_par = sampling of total particles from gamma distribution, y.hat = the predicted difference (CRN-Met).

4.3.4 Snow HBayeRGC: Linear Regression Component

The snow HBayeRGC model's linear regression component is structured as follows:

```
y.hat[i] <- b0 + b1 * truexs_int[i] + b2 * truexs_par[i] +
    b3 * truexs_dur[i] + b4 * truexs_ved[i] +
    b24 * truexs_par[i] * truexs_ved[i] +
    b12 * truexs_int[i] * truexs_par[i]}}
```

Equation 5

where, b0 = intercept coefficient, b1 = intensity coefficient, b2 = total particles coefficient, b3 = duration coefficient, b4 = VED coefficient, b24 = total particles*VED interaction coefficient, b12 = intensity*total particles interaction coefficient, truexs_ved = sampling of VED from gamma distribution, truexs_int = sampling of intensity from gamma distribution, truexs_dur = sampling of duration from gamma distribution, truexs_par =

sampling of total particles from gamma distribution, y.hat = the predicted difference (CRN-Met).

Table 4-5: Table 5: Rain JAGS model coefficients table showing the mean, standard deviation, confidence intervals, and Rhat chain convergence. Coefficients are valid for the scaled dataset.

	mean	sd	2.5%	25%	50%	75%	97.5%	Rhat
b0	0.007869	0.353544	-0.673420	-0.294602	0.111717	0.285234	0.505850	1.203187
b1	-2.005291	0.856349	-3.863104	-2.540137	-2.003506	-1.499940	-0.218936	1.698077
b2	2.178737	3.554752	-3.217898	-0.812825	1.483614	5.935629	8.199749	2.860011
b24	-0.327629	1.010335	-1.995390	-1.501407	-0.030077	0.487545	1.013126	2.952733
b3	0.657907	0.194817	0.283319	0.523285	0.650951	0.788882	1.052755	1.146123
b4	-0.047658	0.085943	-0.178203	-0.118048	-0.073541	0.031374	0.110834	1.224713

Table 4-6: Table 6: Mixed JAGS model coefficients table showing the mean, standard deviation, confidence intervals, and Rhat chain convergence. Coefficients are valid for the scaled dataset.

	mean	sd	2.5%	25%	50%	75%	97.5%	Rhat
b0	-0.185164	0.164691	-0.486191	-0.294308	-0.187080	-0.076799	0.159160	1.047679
b1	-1.119538	0.412649	-1.779745	-1.370933	-1.191456	-0.956765	-0.046540	1.178299
b2	0.912615	0.588423	-0.169849	0.441511	0.942443	1.352187	2.000688	1.185928
b3	0.507066	0.360733	-0.106406	0.221619	0.446072	0.835025	1.126871	1.114904
b4	0.029783	0.067039	-0.104889	-0.012998	0.030461	0.076578	0.150993	1.032735

Table 4-7: Snow JAGS model coefficients table showing the mean, standard deviation, confidence intervals, and Rhat chain convergence. Coefficients are valid for the scaled dataset.

	mean	sd	2.5%	25%	50%	75%	97.5%	Rhat
b0	-0.896641	1.068503	-4.217480	-1.017994	-0.635836	-0.225640	0.190156	2.152433
b1	-0.049570	0.270668	-0.467097	-0.249075	-0.080390	0.128992	0.481991	1.307479
b12	0.844025	0.294737	0.316056	0.663726	0.829657	1.019989	1.453728	1.218747
b2	1.883407	0.560676	1.107697	1.400273	1.819752	2.260292	3.222806	1.594852
b24	-0.229539	0.053077	-0.345199	-0.262416	-0.218192	-0.193708	-0.149121	1.601563
b3	0.218048	0.063062	0.077372	0.178533	0.223029	0.262229	0.329557	1.048041
b4	0.078200	0.109677	-0.034269	0.008181	0.051009	0.091134	0.421618	2.256298

Rain:

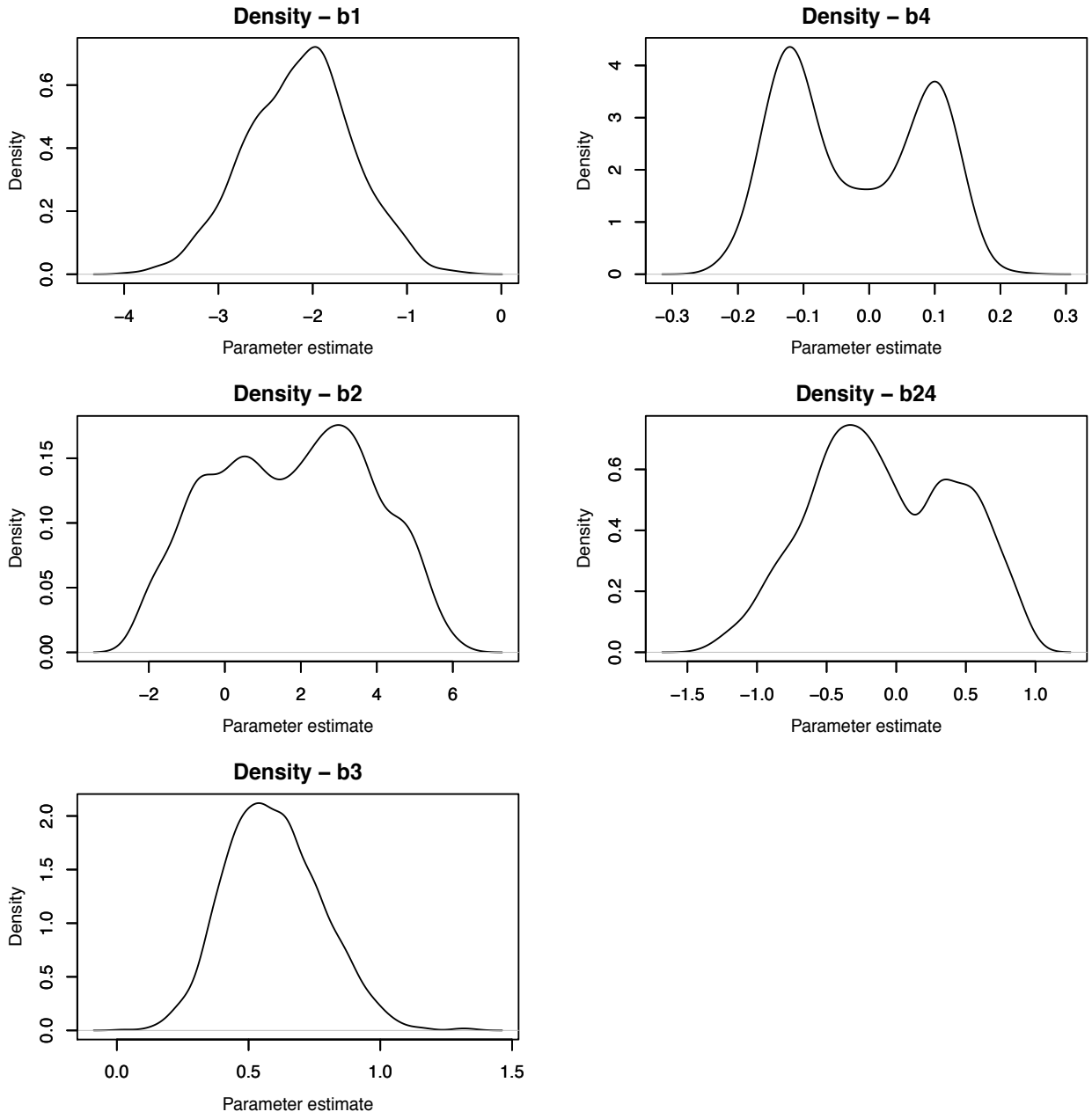

Figure 4-4: Plots of the posterior distributions for the rain HBayeRGC coefficients. b1 = total particles coefficient, b2 = intensity coefficient, b3 = duration coefficient, b4 = wind speed coefficient, b24 = intensity * wind speed interaction coefficient.

Mixed:

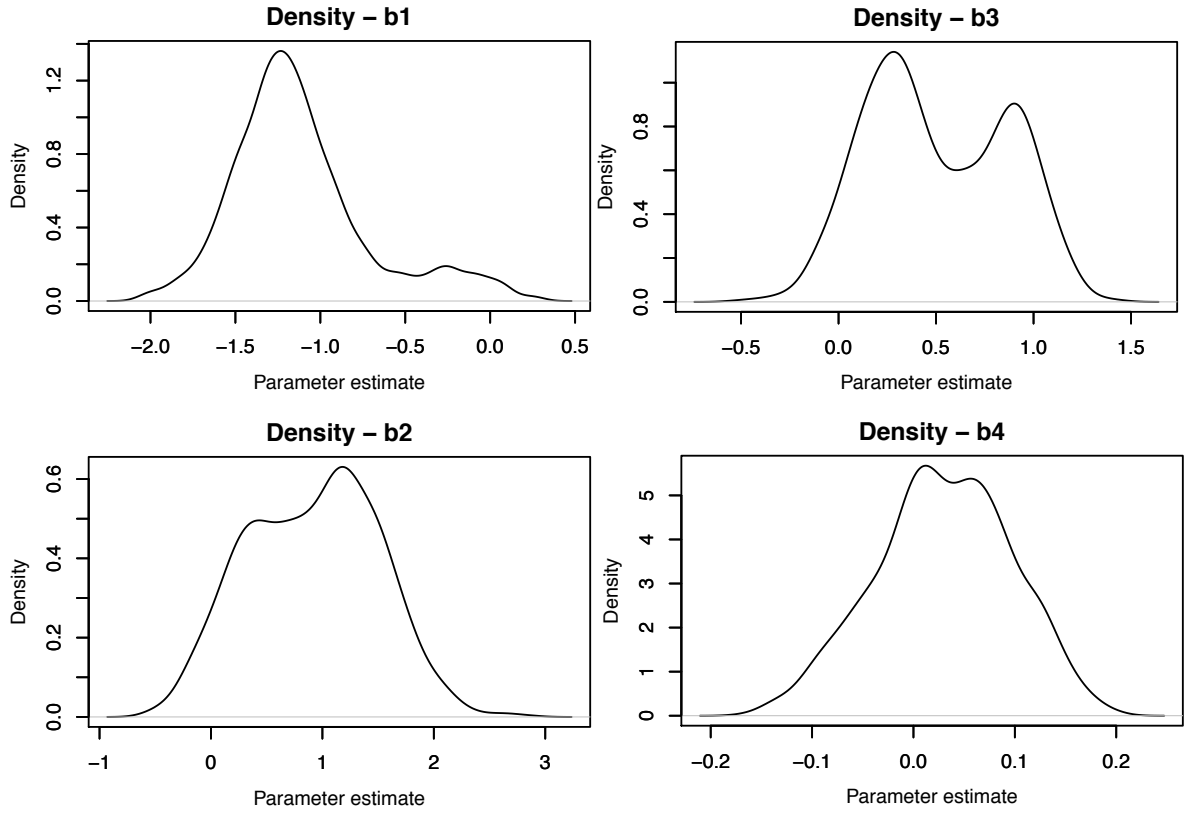

Figure 4-5: Plots of the posterior distributions for the mixed HBayeRGC coefficients. b1 = total particles coefficient, b2 = intensity coefficient, b3 = duration coefficient, b4 = wind speed coefficient

Snow:

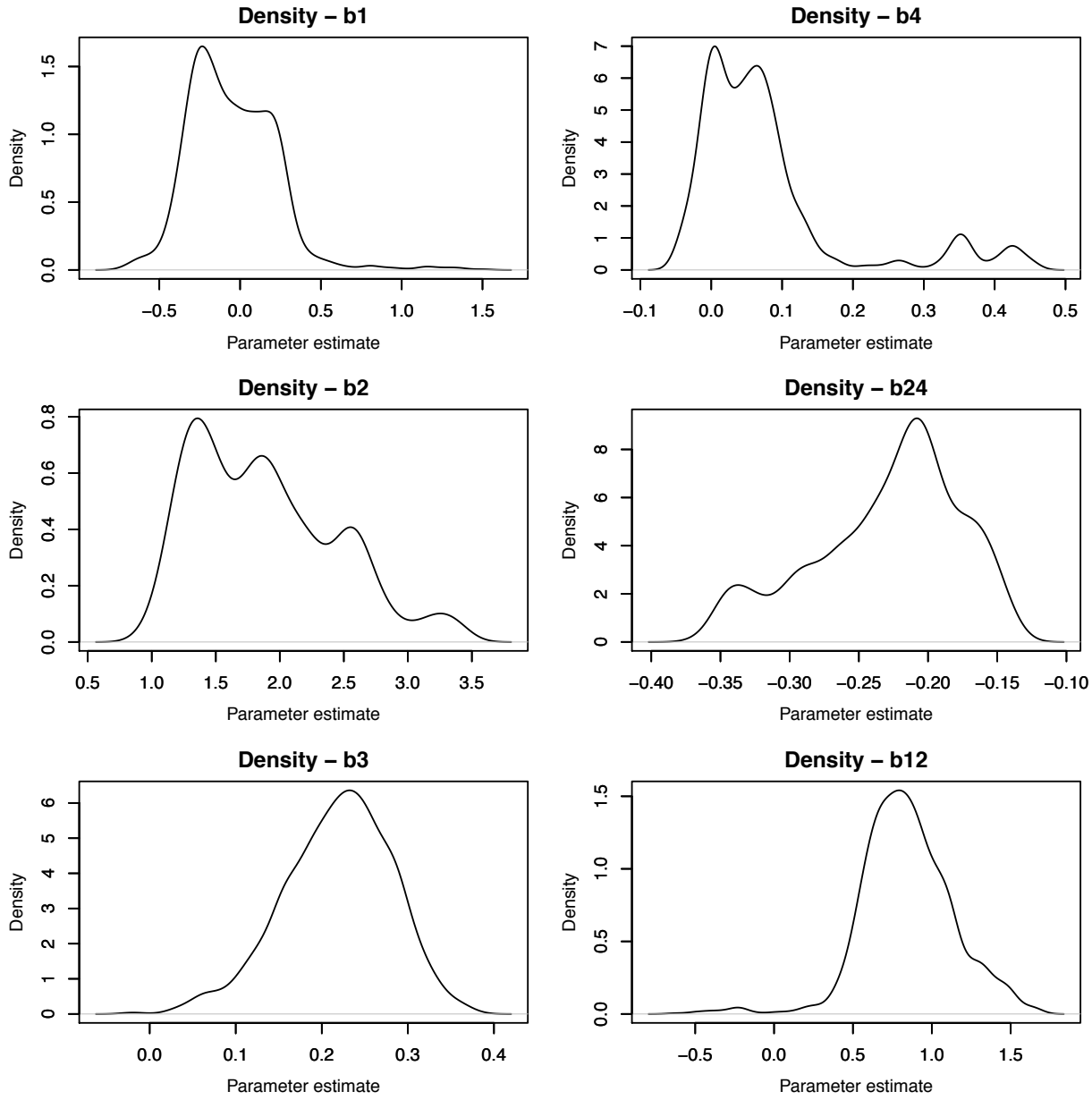

Figure 4-6: Plots of the posterior distributions for the snow HBayeRGC coefficients. b1 = intensity coefficient, b2 = total particles coefficient, b3 = duration coefficient, b4 = VED coefficient, b24 = total particles*VED interaction coefficient, b12 = intensity*total particles interaction coefficient

Chapter 5

Gauge Correction Results

5.1 Overview of results

The HBayeRGC gauge correction model is capable of modeling the accumulation differences between the USCRN reference and the LTER-Geonor unshielded gauge. Furthermore, the HBayeRGC estimates daily uncertainties and identifies periods in the precipitation record with large unknown errors. Although the coefficient posterior distributions are relatively dispersed, the predicted posterior distributions are generally precise (i.e., the estimates are well predicted) and provide reasonable uncertainty information for each daily prediction. The HBayeRGC outperforms recently published gauge correction methods and the multiple linear regression approach. There is similar model performance for rain, mixed, and snow events with the particular combination of environmental conditions likely driving the variation in predictive skill. Including hydrometeor size and count information only slightly improves the HBayeRGC performance but is a significantly better gauge difference predictor than wind speed. The

uncertainty in precipitation accumulation for the LTER-Geonor during the 2013-2014 water year is defined from the HBayeRGC and is among the USCRN total accumulation.

5.2 Coefficient posterior distributions

The coefficient posterior distributions provide a level of confidence in the mean coefficient value selected by the HBayeRGC. All coefficient posteriors are relatively wide with variable PDFs observed (Figs. 4.4, 4.5, 4.6). Bimodal distributions are evident, especially for wind speed in the rain HBayeRGC and duration in the mixed precipitation HBayeRGC, indicating alternative coefficient values are possible. Each explanatory variable has a different effect on predicting the gauge difference between the rain, mixed, and snow models; this is readily seen by comparing the PDF shape of a given variable across the different precipitation type models. In the rain model, the duration coefficient and the total particles coefficient PDF are the closest to a normal distribution; whereas in the mixed-precipitation model, the wind speed is closest to normally distributed with the total particles largely right-skewed. In the snow model, the duration coefficient is also approximately normal and the intensity*total particles interaction coefficient is close to normal but with a large negative left-skewed tail. These PDF shapes, standard deviations of estimated coefficients, and Bayesian MCMC trace convergence criteria, are indications of the strength and direction of, and confidence in the effect each explanatory variable has on the LTER-Geonor errors.

5.3 Response posterior distributions

The HBayeRGC provides uncertainty information for each daily prediction of the gauge differences. Confidence is high in a predicted gauge difference when the MCMC traces have good convergence and the PDF of the parameter estimate is narrow (low standard deviation). Conversely, confidence is low in a predicted gauge difference when the MCMC traces have poor convergence and the PDF of the parameter estimate is wide (high standard deviation). Figure 5.1 shows an example MCMC trace and density plot for low, intermediate, and high standard deviations of the parameter (i.e., predicted gauge difference) estimate. Along with the standard deviation of the parameter estimate providing an uncertainty estimate for the daily predicted gauge difference, the shapes of the PDFs indicate the likelihood of alternative estimates. This information can be used to determine when there are sources of error not included in the HBayeRGC model that have a strong influence on producing an observed gauge difference.

The highly bimodal PDF for the high standard deviation case (Fig. 5.1c) suggests that there are alternative gauge difference predictions; one based on the environmental predictors included in the model and another due to unknown errors. Subsequent investigation into the high standard deviation event reveals that the LTER-Geonor gauge had a one-day lag in recording the large amount of precipitation falling on that particular day (April 3, 2015: USCRN recorded 15.8 mm and LTER recorded 5.4 mm; April 4, 2015: USCRN recorded 4.8 mm and LTER recorded 16.1 mm). Thus, the HBayeRGC predicted a difference near 0 mm given the physical conditions on that day but also predicted the

large observed negative difference (LTER > USCRN) due to capturing underlying but unprescribed errors.

The intermediate standard deviation case (Fig. 5.1b) also identifies a source of gauge differences not specified in the HBayeRGC. In this case, the USCRN did not measure any precipitation whereas the LTER measured 3.4 mm (January 22, 2015). However, the disdrometer indicated that 154,313 hydrometeors fell to the ground on that day. The physically based predicted gauge difference, if the USCRN would have measured the hydrometeors detected by the disdrometer, is likely close to or below 0 mm. Instead the HBayeRGC produced a mean predicted difference of +2.21 mm. This dynamic was detected by the peak near 0 mm but much larger peak near 1 mm (scaled difference) in Figure 5.1-b. Again, the HBayeRGC is capturing unexpected errors not prescribed in the model, but in this case, the error, although small, was associated with the USCRN reference gauge.

An expected undercatchment of precipitation during a moderate snowfall event with strong winds was captured in the low standard deviation case (Fig. 5.1a). On this day, November 10, 2014, the USCRN recorded 7.9 mm of precipitation whereas the LTER-Geonor recorded only 6.7 mm. The mean wind speed for the day was 2.7 m/s (maximum = 8.7 m/s) with 600 minutes of precipitation and a moderate maximum 15-minute precipitation intensity of 0.2 mm/hour. The narrow distribution of the posterior estimate suggests that this type of event was well predicted by the HBayeRGC along with high level of confidence that the environmental conditions responsible for driving the gauge difference was described well in the HBayeRGC model structure.

Large undercatchements of snow during intense snowstorms with high winds were correctly modeled with the HBayeRGC. This is most evident for the November 25, 2014 case when the USCRN measured 18 mm of precipitation and the LTER-Geonor only measured 5 mm of precipitation. The mean windspeed on this day was 9 m/s (maximum wind speed of 11.8 m/s) with 1215 minutes of precipitation, a high maximum 15-minute precipitation intensity of 0.24 mm/hour, and ~ 2 million hydrometeors recorded. The posterior distribution of the predicted difference estimate (Fig. 5.2) demonstrates that the HBayeRGC predicts, with high confidence, a large undercatchment of 12.5 mm of precipitation (actual difference of 13 mm) by the LTER-Geonor during this strong snowstorm.

a.) Low standard deviation (original scaled difference = +0.337 mm):

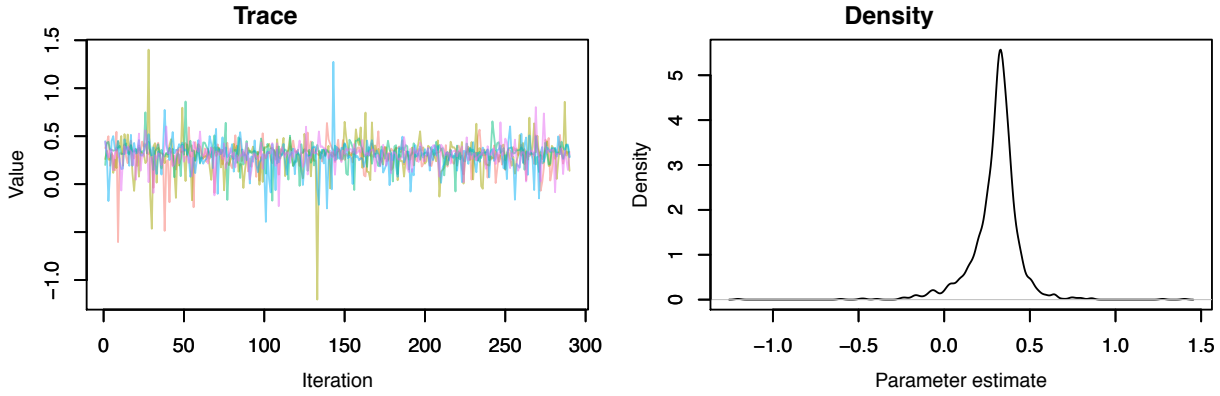

b.) Intermediate standard deviation (original scaled difference = -0.095 mm):

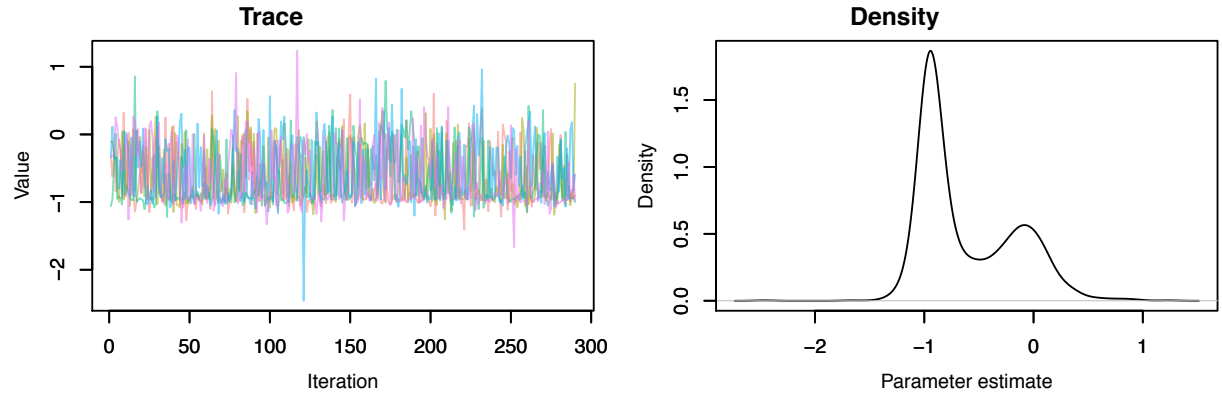

c.) High standard deviation (original scaled difference = -3.174 mm):

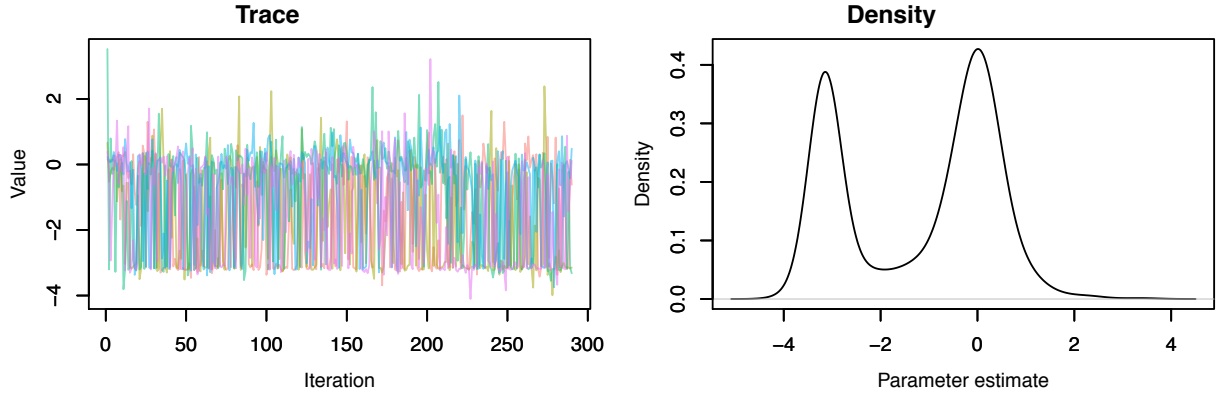

Figure 5-1: Plots of MCMC traces and posterior distributions of low, intermediate, and high dispersion (standard deviation) for 3 snow HBayeRGC predicted differences. Parameter estimates are scaled values.

Intense and long duration snowfall with high winds and 13 mm undercatchment:

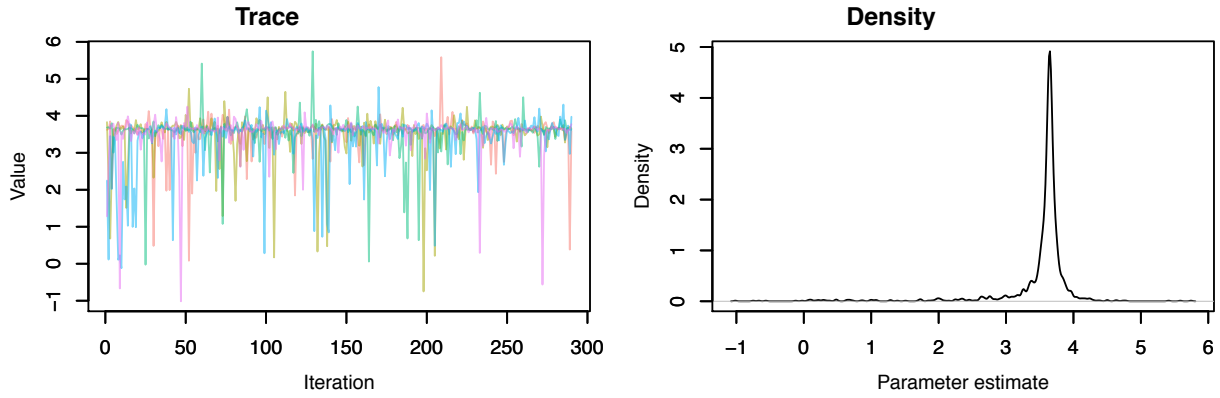

Figure 5-2: Plot of MCMC traces and posterior distributions for a high intensity and long duration snowfall with high winds. The LTER-Geonor recorded 13 mm less precipitation than the USCRN. The HBayeRGC model predicted 12.5 mm undercatchment. Parameter estimates are scaled values.

5.4 Model diagnostics

The HBayeRGC is a significantly better model than published gauge correction methods (Fig. 5.3). To assess the accuracy of the HBayeRGC, we applied a recently developed transfer function derived from the World Meteorological Organization Solid Precipitation InterComparison Experiment (WMO-SPICE; Kochendorfer et al., 2018). We used equation 1 in Kochendorfer et al., 2018 (hereafter: K2018CE):

$$CE = e^{-a(U)\left(1-tan^{-1}\left(b(T_{air})\right)+c\right),} \qquad \text{Equation 6}$$

where CE is the catch efficiency (USCRN/LTER-Geonor), U is mean wind speed (m/s; developed on 30-minute periods), T_{air} is mean air temperature (°C), and a, b, and c are coefficients fit with non-linear-least squares model fitting. The CE was then converted to gauge difference for comparison with the multiple linear regression and hierarchical Bayesian models of the gauge difference. Figure 5.3 demonstrates that K2018CE was thoroughly inadequate at explaining the errors between the USCRN reference and the

unshielded Geonor gauge at the Niwot Ridge C1 subalpine site over the October 1, 2013 to May 12, 2015 comparison period. Applying the K2018CE method resulted in: i) minimal reduction in the root mean square error (RMSE); ii) only a slight increase in the correlation between USCRN and LTER-Geonor corrected with K2018CE; iii) a high mean bias approaching 0.5 mm/day and; iv) an undetectable difference in improving the percentage of errors between -1 and +1 mm/day. This was in stark contrast to the performance of the HBayeRGC (Fig. 5.3).

The HBayeRGC was also a significant improvement over the multiple linear regression (MLR) correction. The MLR model described above and used to develop the HBayeRGC performs better than the K2018CE, except in improving the percentage of errors between -1 and +1 mm/day (Fig. 5.3). The MLR was the best correction model for reducing the overall record mean error and gauge undercatchment (mean bias of $-1.19e^{-15}$) but had less ability than the HBayeRGC to explain and predict daily precipitation errors (Fig. 5.3). With the MLR explaining 48% of the variation in gauge differences (Adj. R^2 for full MLR model of 0.48), it is a reasonable correction method but this is far below the **HBayeRGC's ability to explain 86% of the variation in gauge differences** (Adj. R^2 for the combined rain, mixed, and snow HBayRGCs is 0.86; Fig. 5.4). Furthermore, the MLR's reduction in RMSE is roughly half that of the HBayeRGC's reduction (MLR reduction: 0.92; HBayeRGC reduction: 1.98) and has 45% fewer daily errors between -1 and +1 mm/day (as compared to the HBayeRGC; Fig. 5.3).

Hydrometeor size and count information improved the HBayeRGC and MLR gauge prediction performance and modifies the structure of the gauge correction models. The

relative importance of hydrometeor information in gauge correction models was assessed by comparing models with and without disdrometer data. Model statistics show that there is a slight reduction in model errors when hydrometeor size and count information is included in the model (Fig. 5.3). Furthermore, when selecting the best linear model for snow, windspeed was not a significant model coefficient whereas volume equivalent diameter and total number of particles are highly significant (Particles Total*VED interaction p-value: $8.91e^{-8}$). Additionally, wind speed as a single predictor for snow gauge difference was only marginally significant (p-value 0.055). Thus, hydrometeor characteristics explain more of the variation in the unshielded LTER-Geonor gauge error than wind speed when the precipitation type is snow.

Overall, the model statistics and diagnostics presented here demonstrate that the HBayeRGC is capable of predicting the difference between the USCRN and the LTER-Geonor gauge at the Niwot Ridge C1 site and does far better at doing so than the other methods examined here. The HBayeRGC explained 86% of the variation in the USCRN – LTER-Geonor gauge difference and suggests that more information beyond air temperature/precipitation type and wind speed is required for a skillful gauge correction. In addition to high model performance, the posterior distributions of the model coefficients and daily predicted difference provide valuable uncertainty information that extends the usefulness of the HBayeRGC to unknown error detection and time-dependent uncertainty estimation for a variety of environmental conditions.

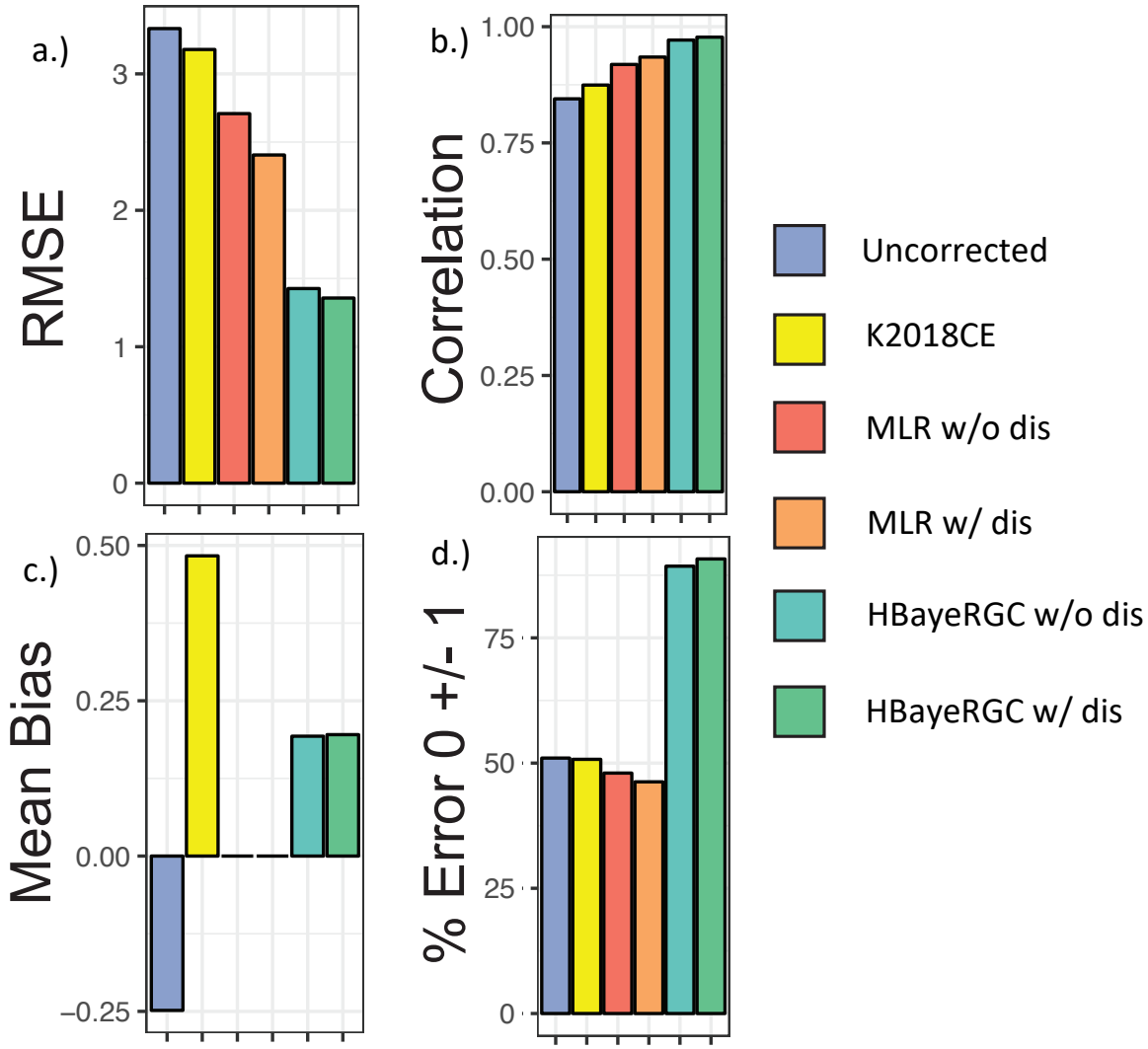

Figure 5-3: Gauge correction model statistics. The difference between the USCRN and LTER-Geonor daily precipitation accumulations are considered the "truth" observation errors/differences. The uncorrected LTER-Geonor is included in purple as a reference value for all modelled values. The non-linear-least-square fitting of the Kochendofer 2018 equation (1) catch efficiency transfer function is in yellow. The multiple linear regression without disdrometer (w/o dis) information is in red. The multiple linear regression with disdrometer (w/ dis) information is in orange. The HBayeRGC model without disdrometer information is in turquois. The HBayeRGC model with disdrometer information is in green. The order of each model in each plot is the same as listed here. Root-mean square error (RMSE) of the observed – predicted differences are shown in (a.). Correlation between observed – predicted differences are shown in (b.). Mean bias (-1*mean) of daily difference between original and predicted accumulation are shown in (c.). The percent of the predicted differences within -1 and +1 of the observed gauge difference are shown in (d.).

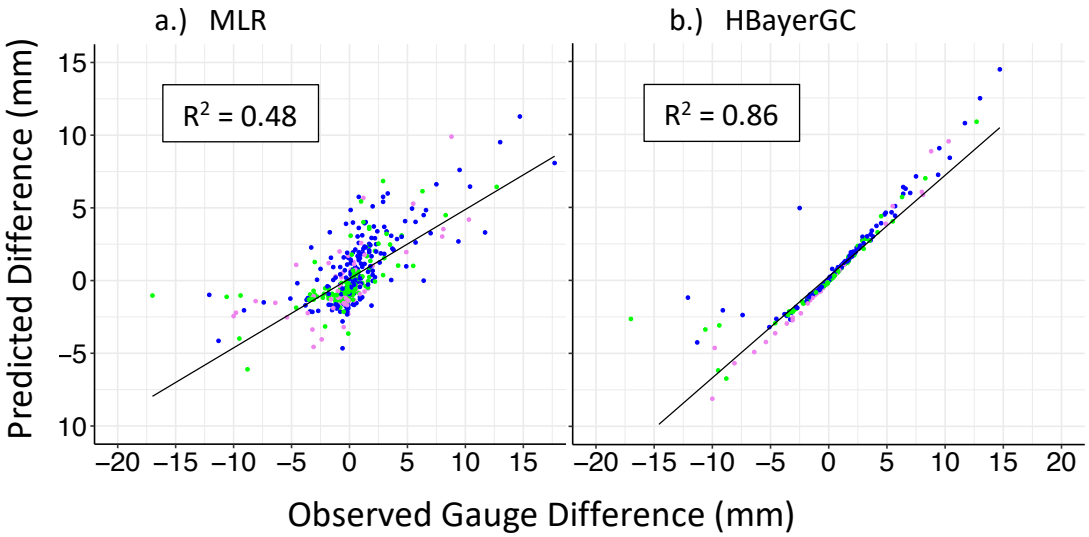

Figure 5-4: Scatter plots of the observed difference (USCRN - LTER-Geonor) and predicted gauge difference for the multiple linear regression (MLR) (a.) and the hierarchical Bayesian regression gauge correction (HBayeRGC) models (b.).

5.5 Daily HBayeRGC performance

The HBayeRGC captures the variability in daily gauge differences throughout the comparison period (Fig. 5.6). Daily original gauge differences demonstrate that there is a systematic LTER-Geonor undercatchment of snow during the winter months, variable but relatively low magnitude over- and undercatchment of rain during the summer/fall months, and highly variable and large over- and undercatchment during the spring "mixed" precipitation period (Fig. 5.6a and Fig. 3-2). The temporal variation in the LTER-Geonor gauge errors are well predicted by the HBayeRGC; predicting both the under- and overcatchment of precipitation (Fig. 5.6b). The largest errors in the LTER-Geonor corrected with HBayeRGC (USCRN – LTER-Geonor-HbayerGC) occur during the spring

when precipitation type is highly variable and allude to this period containing sources of errors not prescribed in the HBayeRGC (Fig. 5.5c).

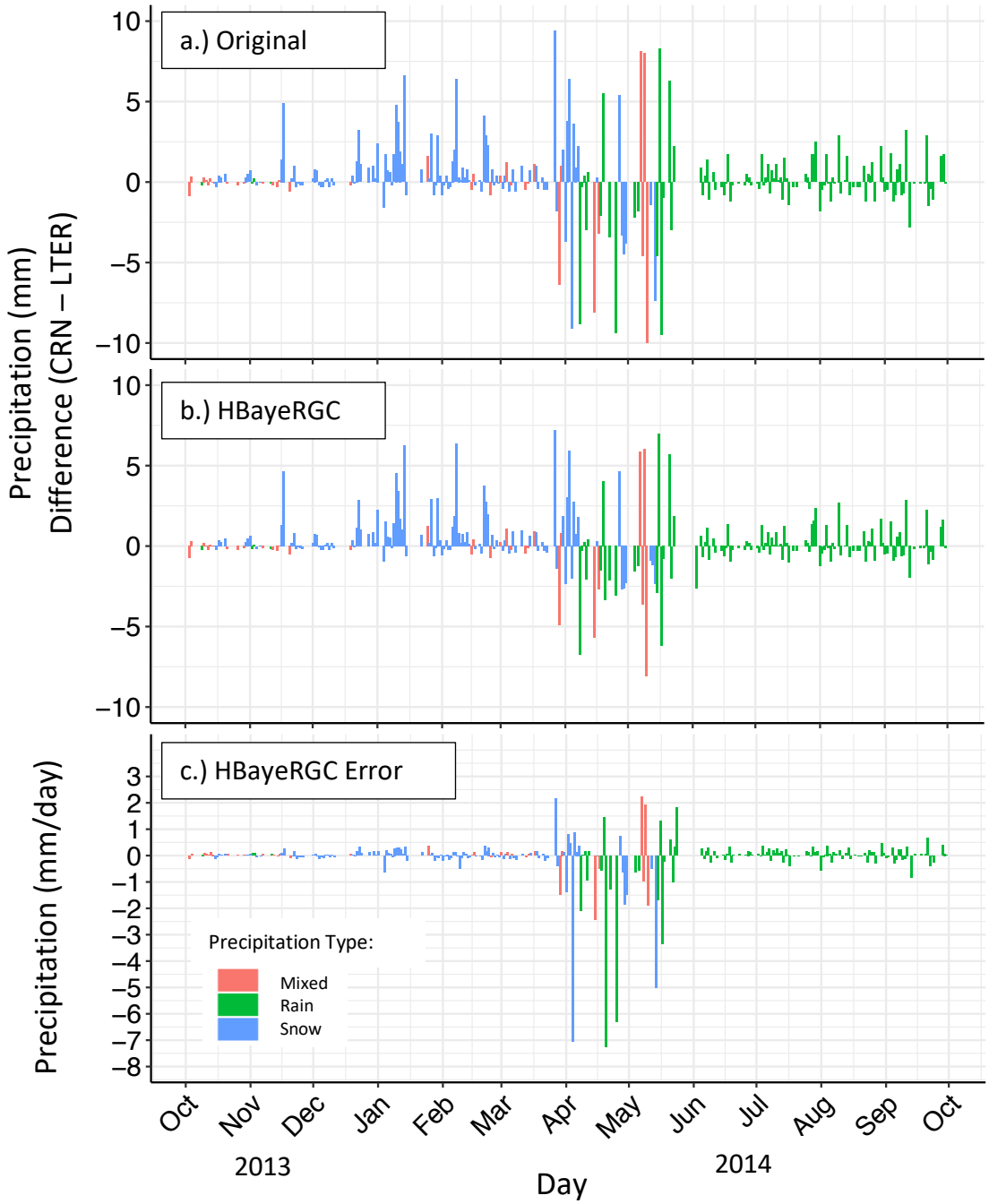

Figure 5-5: The original (a) and HBayeRGC daily difference (USCRN – LTER) (b) in precipitation. The difference between the LTER-Geonor precipitation corrected with the HBayeRGC and the USCRN precipitation (HBayeRGC error) is shown in panel (c.). Excludes differences greater than +10 and less than -10 mm. No data excluded in (c.). Based on 24-hour precipitation totals.

5.6 Daily Uncertainty Estimation

The standard deviation (sd) of the HBayeRGC posterior predicted gauge difference estimates provide a daily estimate of uncertainty in the corrected precipitation record (Fig. 5.6). There is lower confidence (sd > 2 mm) in predicting the larger gauge differences (error > |1| mm) given variation in the magnitude of the standard deviation closely resembling the magnitude variation of the predicted difference. Furthermore, the pattern of daily standard deviation is similar to the pattern of model errors throughout the comparison period and suggests that greater uncertainty in model estimates leads to lower predictability of the HBayeRGC. The daily variation in uncertainty shows that the performance of the HBayeRGC varies at the daily scale and provides an opportunity to investigate the particular set of conditions leading to the likelihood of each predicted gauge difference representing the true difference.

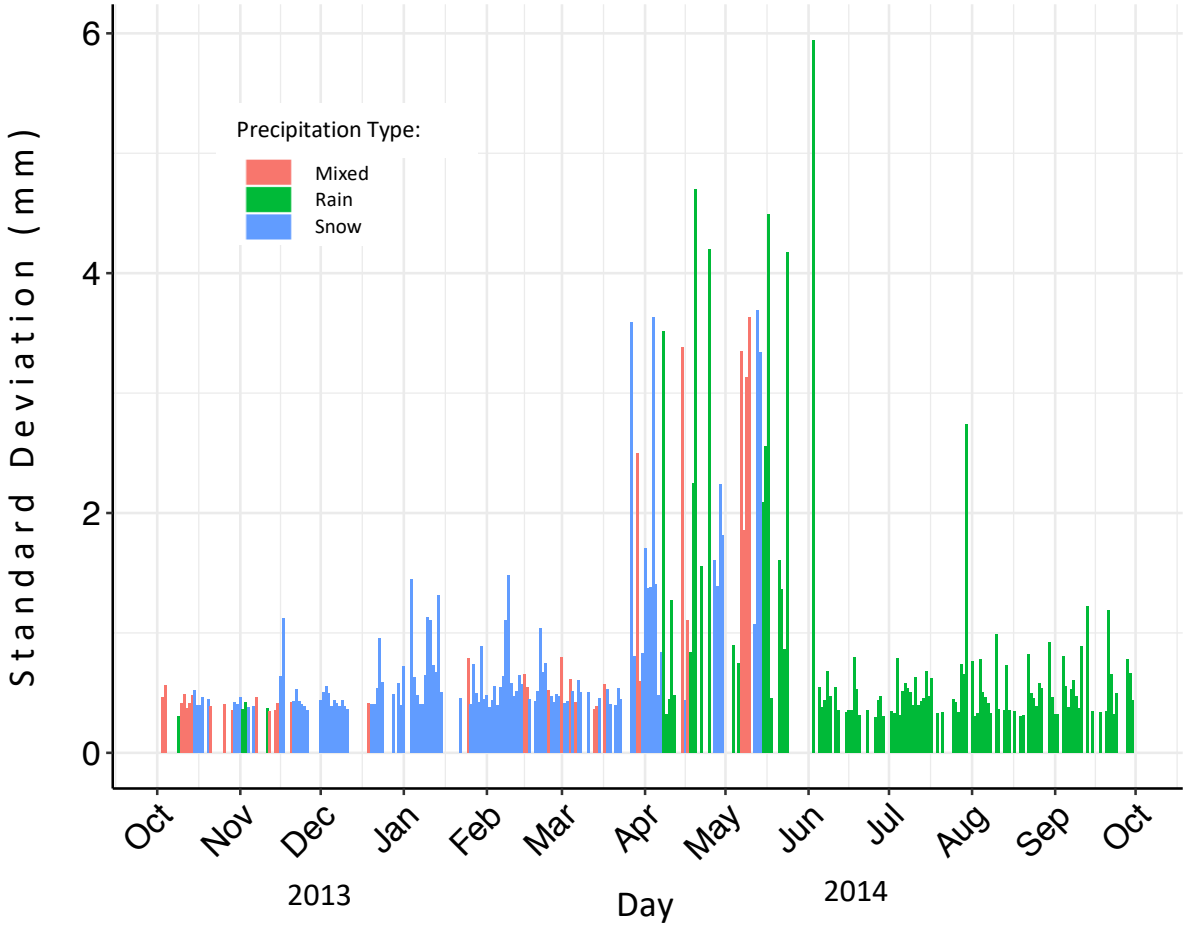

Figure 5-6: Standard deviations of the posterior daily estimate in precipitation error between the USCRN and LTER-Belfort gauge. Based on 24-hour totals.

5.6 Gauge correction

The HBayeRGC corrects the LTER-Geonor precipitation accumulation over the 2013-14 water year, and provides a level of confidence in the corrected record (Fig. 5.7). The range of total precipitation is calculated by accumulating + and – 1 standard deviation of the daily accumulation (derived from HBayeRGC posterior distributions). This results in a total year accumulation for the LTER-Geonor corrected 2013-2014 water year record (gaps removed) between 875 and 1067 mm. The USCRN total precipitation for the same period (identical day gaps removed) was 983 mm; close to half-way between the LTER-Geonor HBayeRGC corrected uncertainty range of +/- 96 mm of precipitation. The variation in accumulation rates between the uncorrected, HBayeRGC corrected, and the USCRN provide insight into the performance of the HBayeRGC throughout the water year. For this particular 2013-2014 water year comparison, the USCRN reference accumulation is within the LTER-Geonor HBayeRGC corrected accumulation; however, there are periods when the USCRN accumulation is near the maximum of the corrected accumulated range. This variation in daily difference between the USCRN and LTER-Geonor HBayeRGC corrected record allows the HBayeRGC model to be assessed for under- or overcatchement performance on a daily and seasonal basis. Overall, the results here demonstrate that the HBayeRGC method is a capable of producing a physically based and defensible, due to uncertainty estimation, correction of the unshielded Geonor gauge located at the Niwot Ridge LTER C1 subalpine site.

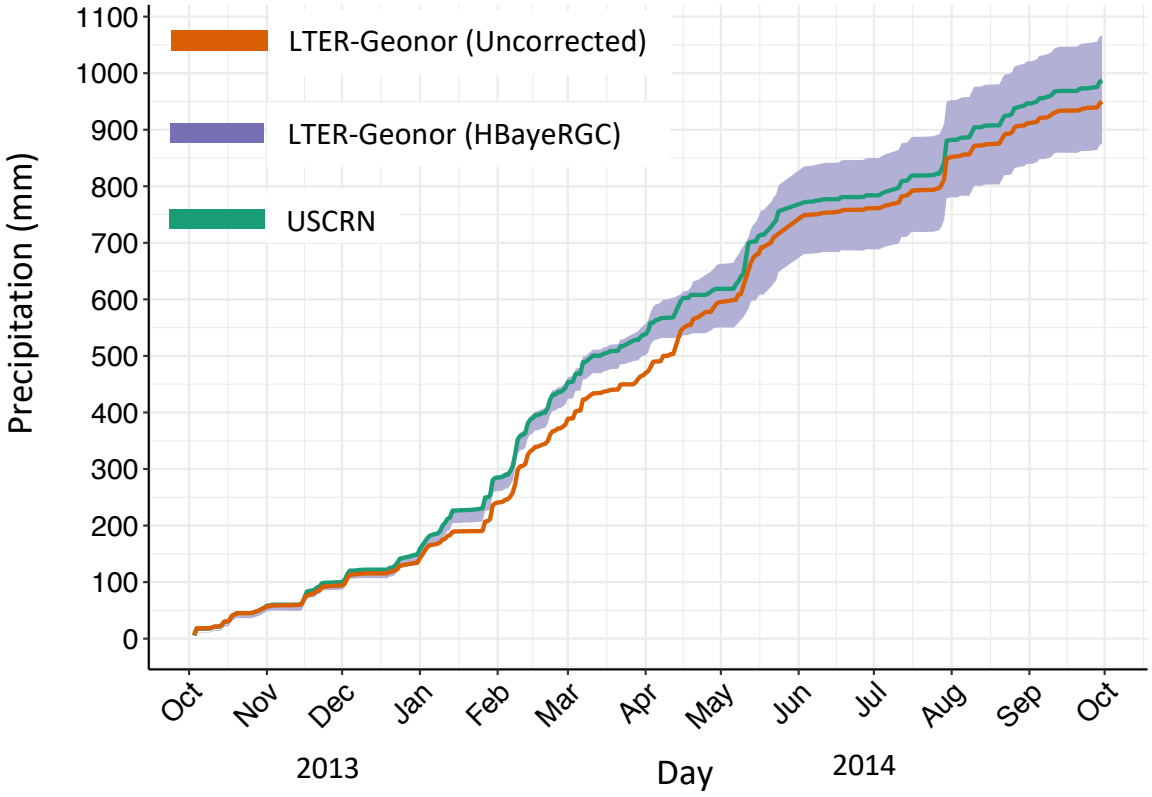

Figure 5-7: The 2013-2014 water year precipitation accumulation (mm) for the USCRN (green) and the HBayeRGC corrected LTER-Geonor with +/- standard deviation (purple). Standard deviations are generated from the Bayesian posterior distributions for each predicted daily gauge difference (USCRN minus LTER-Geonor). Accumulations are not adjusted for gaps.

Chapter 6

Discussion

In this thesis, we have shown that the Hierarchical Bayesian Regression Gauge Correction (HBayeRGC) model is an improved and valuable approach to correcting an unshielded and error-prone gauge in a windy mountain environment. Assessing the predictive ability of the HBayeRGC revealed that gauge differences between the U.S. Climate Reference Network's (small) double fence intercomparison reference (USCRN sDFIR) gauge and the Niwot Ridge LTER's unshielded, but same brand and model, gauge (LTER-Geonor) can be reasonably predicted despite both under- and overcatchment accumulation errors. The linear regression model selection process exposed the combination of explanatory variables, including interactions between them, that best describes the differences between the USCRN and LTER-Geonor gauge (USCRN minus LTER-Geonor) during rain, mixed-phase, and snow events. Bayesian posterior distributions of the model coefficients (Figs. 4-4, 4-5, and 4-6) provide a range and confidence interval of the explanatory estimate values that contribute to understanding the relative importance and effect of each component of the gauge correction model. The

predicted gauge difference posterior distributions (examples in Figs. 5-1 and 5-2) expose the uncertainty in predicted differences for a given set of physical conditions (wind speed, precipitation intensity, hydrometeor size, counts, and type, and duration of precipitation) and uncover large errors (> +/- 1 mm/day) not prescribed in the HBayeRGC. Detection of unknown errors, that could be due instrument malfunctions or related to the difference in forest canopy structure between gauge locations, suggests that the HBayeRGC can be used as an iterative data filtering and model reformulation method that minimizes predicted gauge difference uncertainty. The fact that the HBayeRGC explains 86% of the variation of the observed gauge difference and explains 38% more than the MLR is a good indication of the high predictability of gauge errors using this approach. A range of probable gauge errors are produced by modelling gauge errors with Bayesian likelihoods formulated from estimations of site-specific probability distributions of the explanatory estimates. Predicting gauge errors in this way is significantly better than other approaches that developed catch efficiency (reference/unshielded) functions at highly controlled comparison sites for the purpose of applying the corrections at many sites. The reality is, especially for mountainous sites, that the terrain complexity and remoteness produce more errors with greater magnitude that are specific to each site. A successful gauge correction in complex terrain, therefore, requires that all the available and potentially useful information, including probability distributions of that information, at the site of interest are used. The HBayeRGC developed and describe here in this thesis demonstrates, through significant reduction in the root mean square error (RMSE) of the

observed to predicted gauge differences, that this is reasonable way forward for gauge corrections in windy mountainous locations.

Hydrometeor characteristics play a significant role in predicting the difference in accumulated precipitation between the USCRN and LTER-Geonor. This was readily apparent in the highly significant p-values for number of particles and volume equivalent diameter coefficients in the multiple linear regression (MLR) model (Table. 1). When the MLR was split up between times with rain, mixed-phase precipitation, and snow, wind speed was not a significant predictor in the snow events but hydrometeor volume equivalent diameter (VED) and the number of hydrometeors (including interactions with VED and intensity) were significant predictors. This suggests that the information contained within the VED and number of particles explains more of the variation in gauge differences than wind speed during snowfall events. In other words, measuring hydrometeor characteristics is more important than measuring wind speed when attempting to discern gauge errors. This could be due to a large range of influences at low wind speeds from the wide variation in frozen hydrometeor shapes and sizes; a possible future analysis with the data sets described here. The importance of hydrometeor information is confirmed by the reduction in RMSE and the increase in correlation between observed and corrected daily accumulations when disdrometer data (i.e., hydrometeor information) are included in both the MLR and HBayeRGC models (Fig. 5-3a,b). Interestingly, the MLR has an increase in errors less than -1 and + 1 mm/day whereas the HBayeRGC has a decrease in errors less than -1 and +1 mm/day with hydrometeor information suggesting that the HBayeRGC is better equipped to use

hydrometeor information for a better gauge difference prediction (Fig. 5.3d). However, the only slight relative improvement in model performance indicates that reasonable correction models could be developed without disdrometer data. Overall, these results confirm the importance of hydrometeor characteristics in driving gauge errors and advocate for including them in gauge correction models during snowfall events.

The seasonal dynamics of the LTER-Geonor errors are captured with the daily performance of the HBayeRGC. The ability of the HBayeRGC to predict both under- and overcatchment of precipitation is easily seen in 2013-2014 water year daily precipitation plot of the original and predicted differences (Fig. 5.5a,b) and is a critical quality of the method given most precipitation gauge corrections assume an undercatchment of the DFIR reference gauge. The errors in prediction shown in Fig. 5.5c show that HBayeRGC picks up on and adequately predicts the gauge differences during all major and minor snowstorms during the October 2013 through mid-March 2014 period and does a similarly good job at predicting rainfall errors between June 2014 and October 2014. However, there were large and highly variable observed gauge differences during the mid-April 2014 through mid-June 2014 period that produce the largest errors in the HBayeRGC. This period of large model errors corresponds to predicted estimates with wide posterior probability distributions (see Fig. 5.1c for example) suggesting that the sources of the observed gauge differences are not well described in model. The bimodality of the posterior distribution in Fig. 5.1c illustrates the skill HBayeRGC has in detecting alternative predictions; in this case, the HBayerGC's explanatory variables generate a density peak near 0 mm but also are able to capture a large overcatchement of snow with

the density peak near -3 mm (scaled value). This ability of the HBayeRGC to capture alternative predictions explains how the HBayeRGC is able to describe seasonal pattern of these unexpected gauge differences and in doing so, endows the HBayeRGC method with the capability to find and filter gauge errors that are beyond what is described in the model.

The HBayeRGC demonstrates the value in producing likelihood estimates generated from estimated probability distributions, given available observations, of the true explanatory conditions and prior information, in this case the MLR, that forms our gauge error hypotheses. By casting the precipitation gauge errors in terms of likelihood, the HBayeRGC is able to generate uncertainty estimation at the daily scale that is dependent on the set of explanatory conditions described in the model. The standard deviation values in Fig. 5.6 represent the *relative* likelihood of a given predicted gauge difference (hypothesis) of being true. From these standard deviations of the posterior estimates, we see that the least likely predicted gauge differences correspond to the largest HBayeRGC model errors and lowest gauge difference predictability. Therefore, we can reasonably assign uncertainty estimates to each daily predicted gauge estimate and have confidence that the uncertainty is a reflection of the unique combination of explanatory conditions and unknown sources of errors. For example, with a R^2 of 0.86 for the modelled October 1, 2013 to May 12, 2015 gauge comparison period for which the HBayeRGC was developed on, the remaining 14% of the variation can be assigned as a frequentist (vs Bayesian) random error term across the entire period. The correctly modelled 86% of the variation, however, is assigned a daily uncertainty estimation that can be viewed as the probability

of the of corrected gauge value representing the true gauge value as determined by the USCRN DFIR gauge. In the context of the accumulated precipitation, the magnitude of the total precipitation for that day in combination with HBayeRGC explanatory posterior distributions can be used to determine the likelihood of obtaining a correction close to the "truth" and can be used in conjunction with a gauge correction to estimate uncertainty on the entire C1 precipitation record.

The motivating goal of this work was to produce a precipitation gauge correction that outperforms currently published corrections in a less than ideal gauge comparison environment. With the highly predictive HBayeRGC outperforming, on all model diagnostics (Fig. 5-3), the best available correction function developed from WMO-SPICE gauge comparisons (K2018CE) and a reasonable correction of the unshielded LTER-Geonor gauge during the comparison period (Fig. 5-7) despite variable over- and undercatchment errors, variable forest canopy structure between gauge locations influencing interception of snow, and potentially unforeseen data quality issues, we have achieved our goal. Perhaps more importantly, this thesis has developed an approach to precipitation gauge corrections that can be adapted to the suite of available data sets and instrumentation at specific sites. For instance, the HBayeRGC can be used as is with new USCRN and disdrometer data and the predictive skill can be assessed. However, the best gauge correction for a new site or extending the correction for the Niwot Ridge C1 record back to 1952, will require assimilating a new set of available meteorological information for that period, formulating the best possible MLR model, and determining probability distributions of the best available explanatory information before running a period or site

specific HBayeRGC (see Chapter 4.3.1 and Appendix A for detailed steps on how to implement the HBayeRGC for a variety of situations). The latter, once reasonable gap-filling methods have been applied, is the logical next application of the HBayeRGC model for the Niwot Ridge subalpine precipitation record. The HBayeRGC is therefore a flexible method, not a site-specific transfer function, that can be applied at any site, so that the best possible gauge corrections and uncertainty estimation in complex mountain terrain can be achieved.

The comparison of MLR and HBayeRGC models with and without hydrometeor size and count information demonstrates that the best possible correction is achieved by including disdrometer information. Although snow MLR model explains 7% more of the variation in gauge differences and the HBayeRGC performs slightly better on all model diagnostics (Fig. 5-3) with disdrometer information, the relatively small improvement in model improvement suggests that a reasonable gauge correction can be achieved without a disdrometer. However, since the MLR model selection process for the snow precipitation type determined that wind speed is not a significant predictor (p-value = 0.3) of gauge differences when hydrometeor information is included, we infer that hydrometeor information is more important than wind speed information in explaining the difference in snow accumulation between the USCRN reference and the LTER-Geonor unshielded gauge. These results make sense in light of the disdrometer providing a greater degree of information than the anemometer but based on gauge airflow modelling, prior gauge corrections, and the MLR and HBayeRGC without disdrometer information, wind speed is a proven predictor of gauge errors.

Chapter 7

Conclusion

Sub-daily wind speed, precipitation intensity and duration, hydrometeor diameter and count information are incorporated into a hierarchical Bayesian regression model (HBayeRGC) to develop a gauge correction model that is capable of explaining 86% of the variation in gauge differences between the USCRN DFIR and an unshielded Geonor gauge at the Niwot Ridge C1 subalpine site. The HBayeRGC is based on data from the October 1, 2013 to May 12, 2015 period that had minimal gaps in the unshielded gauge record and overlapped with an OTT Parsivel disdrometer operating at the site. This is the first study we are aware of to incorporate continuously recorded hydrometeor information into a precipitation gauge correction. Including hydrometeor information slightly improved gauge difference predictions but is not enough of an improvement to warrant a strong recommendation to include disdrometer data in future site-specific precipitation gauge corrections. However, hydrometeor volume equivalent diameter and count model variables explain significantly more of the gauge difference variation than wind speed when precipitation type is snow and confirms that the physical aspects of frozen

hydrometeors are relevant for understanding the sources of gauge errors and may contribute valuable gauge correction uncertainty information. Bayesian inference was used to model unique probability distributions of the explanatory meteorological data and in turn produced daily precipitation gauge uncertainty estimates that can be used to detect gauge errors not prescribed in the correction model. Despite the low correlations between single explanatory variables and gauge differences, the HBayeRGC is a highly predictive gauge correction model for the comparison period that provides insights into the explanatory power of a combination of meteorological information. The HBayeRGC provides a *method* to extend the correction and uncertainty estimates to the entire Niwot Ridge C1 subalpine precipitation record and can be applied to other gauge comparison sites to understand and correct precipitation gauge errors in a variety of environments.

Achieving more accurate precipitation accumulation records in mountain environments will lead to better predictions of mountain water resources in a changing and highly variable climate. Currently many predicted orographic processes, such as the seeder-feeder orographic enhancement of snowfall (Mott et al., 2014) and the preferential deposition of snowfall on windward vs leeward slopes as a function wind-induced hydrometeor trajectories (Lehning et al., 2008) cannot be quantified due to lack of quality precipitation observations in mountainous terrain. Beyond the large spatial gaps in mountain meteorological stations, especially in the alpine zones which may require a rethinking of measurement techniques, the lack of quality precipitation measurements is partly due to the uncertainty of currently operating gauges (Serreze et al., 1999). The uncertainties in precipitation accumulation in mountainous terrain need to be known,

estimated, and corrected for at high temporal resolution in order to link synoptic scale atmospheric conditions and storm dynamics with the filling of our mountain water towers.

References

Bales, R. C., Molotch, N. P., Painter, T. H., Dettinger, M. D., Rice, R. and Dozier, J.: Mountain hydrology of the western United States, Water Resour. Res., 42(8), doi:10.1029/2005WR004387, 2006.

Battaglia, A., Rustemeier, E., Tokay, A., Blahak, U. and Simmer, C.: PARSIVEL Snow Observations: A Critical Assessment, J. Atmos. Oceanic Technol., 27(2), 333–344, doi:10.1175/2009JTECHA1332.1, 2010.

Blanken, P. D., Williams, M. W., Burns, S. P., Monson, R. K., Knowles, J., Chowanski, K. and Ackerman, T.: A comparison of water and carbon dioxide exchange at a windy alpine tundra and subalpine forest site near Niwot Ridge, Colorado, Biogeochemistry, 95(1), 61–76, doi:10.1007/s10533-009-9325-9, 2009.

Cane, D., Barbarino, S., Renier, L. A. and Ronchi, C.: Regional climate models downscaling in the Alpine area with multimodel superensemble, Hydrol. Earth Syst. Sci., 17(5), 2017–2028, doi:10.5194/hess-17-2017-2013, 2013.

Chen, R., Liu, J., Kang, E., Yang, Y., Han, C., Liu, Z., Song, Y., Qing, W. and Zhu, P.: Precipitation measurement intercomparison in the Qilian Mountains, north-eastern Tibetan Plateau, The Cryosphere, 9(5), 1995–2008, doi:10.5194/tc-9-1995-2015, 2015.

Colli, M., Lanza, L. G., Rasmussen, R. and Thériault, J. M.: The Collection Efficiency of Shielded and Unshielded Precipitation Gauges. Part I: CFD Airflow Modeling, J. Hydrometeor., 17(1), 231–243, doi:10.1175/JHM-D-15-0010.1, 2016a.

Colli, M., Lanza, L. G., Rasmussen, R. and Thériault, J. M.: The Collection Efficiency of Shielded and Unshielded Precipitation Gauges. Part II: Modeling Particle Trajectories, J. Hydrometeor., 17(1), 245–255, doi:10.1175/JHM-D-15-0011.1, 2016b.

Dai, A.: Precipitation Characteristics in Eighteen Coupled Climate Models, J. Climate, 19(18), 4605–4630, doi:10.1175/JCLI3884.1, 2006.

Daly, C., Slater, M. E., Roberti, J. A., Laseter, S. H. and Swift, L. W.: High-resolution precipitation mapping in a mountainous watershed: ground truth for evaluating uncertainty in a national precipitation dataset, International Journal of Climatology, 37, 124–137, doi:10.1002/joc.4986, 2017.

Dettinger, M.: Impacts in the third dimension, Nature Geosci, 7(3), 166–167, doi:10.1038/ngeo2096, 2014.

Dettinger, M., Redmond, K. and Cayan, D.: Winter Orographic Precipitation Ratios in the Sierra Nevada—Large-Scale Atmospheric Circulations and Hydrologic Consequences, J. Hydrometeor, 5(6), 1102–1116, doi:10.1175/JHM-390.1, 2004.

Diodato, N.: The influence of topographic co-variables on the spatial variability of precipitation over small regions of complex terrain, Int. J. Climatol., 25(3), 351–363, doi:10.1002/joc.1131, 2005.

Frei, C. and Scha, C.: A precipitation climatology of the Alps from high-resolution rain-gauge observations, Int. J. Climatol., 28, 1998.

Friedrich, K., Higgins, S., Masters, F. J. and Lopez, C. R.: Articulating and Stationary PARSIVEL Disdrometer Measurements in Conditions with Strong Winds and Heavy Rainfall, Journal of Atmospheric and Oceanic Technology, 30(9), 2063–2080, doi:10.1175/JTECH-D-12-00254.1, 2013.

Gerber, F., Besic, N., Sharma, V., Mott, R., Daniels, M., Gabella, M., Berne, A., Germann, U. and Lehning, M.: Spatial variability in snow precipitation and accumulation in COSMO–WRF simulations and radar estimations over complex terrain, The Cryosphere, 12(10), 3137–3160, doi:10.5194/tc-12-3137-2018, 2018.

Gerber, F., Mott, R. and Lehning, M.: The Importance of Near-Surface Winter Precipitation Processes in Complex Alpine Terrain, J. Hydrometeor., 20(2), 177–196, doi:10.1175/JHM-D-18-0055.1, 2019.

Goodison, B. E., Louie, P. Y. T. and Yang, D.: WMO Solid Precipitation Measurement Intercomparison--Final Report, World Meteorological Organization - Instruments and Observing Methods, 67, 318, 1998.

Greenland, D.: The Climate of Niwot Ridge, Front Range, Colorado, U.S.A., Arctic and Alpine Research, 21(4), 380, doi:10.2307/1551647, 1989.

Herrnegger, M., Senoner, T. and Nachtnebel, H.-P.: Adjustment of spatio-temporal precipitation patterns in a high Alpine environment, Journal of Hydrology, 556, 913–921, doi:10.1016/j.jhydrol.2016.04.068, 2018.

Kittel, T. G. F., Williams, M. W., Chowanski, K., Hartman, M., Ackerman, T., Losleben, M. and Blanken, P. D.: Contrasting long-term alpine and subalpine precipitation trends in a

mid-latitude North American mountain system, Colorado Front Range, USA, Plant Ecology & Diversity, 8(5–6), 607–624, doi:10.1080/17550874.2016.1143536, 2015.

Knowles, J. F., Burns, S. P., Blanken, P. D. and Monson, R. K.: Fluxes of energy, water, and carbon dioxide from mountain ecosystems at Niwot Ridge, Colorado, Plant Ecology & Diversity, 8(5–6), 663–676, doi:10.1080/17550874.2014.904950, 2015.

Kochendorfer, J., Nitu, R., Wolff, M., Mekis, E., Rasmussen, R., Baker, B., Earle, M. E., Reverdin, A., Wong, K., Smith, C. D., Yang, D., Roulet, Y.-A., Buisan, S., Laine, T., Lee, G., Aceituno, J. L. C., Alastrué, J., Isaksen, K., Meyers, T., Brækkan, R., Landolt, S., Jachcik, A. and Poikonen, A.: Analysis of single-Alter-shielded and unshielded measurements of mixed and solid precipitation from WMO-SPICE, Hydrol. Earth Syst. Sci., 21(7), 3525–3542, doi:10.5194/hess-21-3525-2017, 2017a.

Kochendorfer, J., Rasmussen, R., Wolff, M., Baker, B., Hall, M. E., Meyers, T., Landolt, S., Jachcik, A., Isaksen, K., Brækkan, R. and Leeper, R.: The quantification and correction of wind-induced precipitation measurement errors, Hydrol. Earth Syst. Sci., 21(4), 1973–1989, doi:10.5194/hess-21-1973-2017, 2017b.

Kochendorfer, J., Nitu, R., Wolff, M., Mekis, E., Rasmussen, R., Baker, B., Earle, M. E., Reverdin, A., Wong, K., Smith, C. D., Yang, D., Roulet, Y.-A., Meyers, T., Buisan, S., Isaksen, K., Brækkan, R., Landolt, S. and Jachcik, A.: Testing and development of transfer functions for weighing precipitation gauges in WMO-SPICE, Hydrol. Earth Syst. Sci., 22(2), 1437–1452, doi:10.5194/hess-22-1437-2018, 2018.

Langousis, A., Deidda, R., Carsteanu, A. A., Onof, C., Burlando, P., Uijlenhoet, R. and Bárdossy, A.: Precipitation measurement and modelling: Uncertainty, variability, observations, ensemble simulation and downscaling, Journal of Hydrology, 556, 824–826, doi:10.1016/j.jhydrol.2017.09.016, 2018.

Lehning, M., Löwe, H., Ryser, M. and Raderschall, N.: Inhomogeneous precipitation distribution and snow transport in steep terrain, Water Resour. Res., 44(7), doi:10.1029/2007WR006545, 2008.

Lundquist, J. D., Hughes, M., Henn, B., Gutmann, E. D., Livneh, B., Dozier, J. and Neiman, P.: High-Elevation Precipitation Patterns: Using Snow Measurements to Assess Daily Gridded Datasets across the Sierra Nevada, California*, Journal of Hydrometeorology, 16(4), 1773–1792, doi:10.1175/JHM-D-15-0019.1, 2015.

Michaelides, S., Levizzani, V., Anagnostou, E., Bauer, P., Kasparis, T. and Lane, J. E.: Precipitation: Measurement, remote sensing, climatology and modeling, Atmospheric Research, 94(4), 512–533, doi:10.1016/j.atmosres.2009.08.017, 2009.

Mott, R., Scipión, D., Schneebeli, M., Dawes, N., Berne, A. and Lehning, M.: Orographic effects on snow deposition patterns in mountainous terrain, J. Geophys. Res. Atmos., 119(3), 1419–1439, doi:10.1002/2013JD019880, 2014.

Napoli, A., Crespi, A., Ragone, F., Maugeri, M. and Pasquero, C.: Variability of orographic enhancement of precipitation in the Alpine region, Sci Rep, 9(1), 13352, doi:10.1038/s41598-019-49974-5, 2019.

Peleg, N., Ben-Asher, M. and Morin, E.: Radar subpixel-scale rainfall variability and uncertainty: lessons learned from observations of a dense rain-gauge network, Hydrol. Earth Syst. Sci., 17(6), 2195–2208, doi:10.5194/hess-17-2195-2013, 2013.

Rasmussen, R., Baker, B., Kochendorfer, J., Meyers, T., Landolt, S., Fischer, A. P., Black, J., Thériault, J. M., Kucera, P., Gochis, D., Smith, C., Nitu, R., Hall, M., Ikeda, K. and Gutmann, E.: How Well Are We Measuring Snow: The NOAA/FAA/NCAR Winter Precipitation Test Bed, Bull. Amer. Meteor. Soc., 93(6), 811–829, doi:10.1175/BAMS-D-11-00052.1, 2011.

Rasouli, K., Hsieh, W. W. and Cannon, A. J.: Daily streamflow forecasting by machine learning methods with weather and climate inputs, Journal of Hydrology, 414–415, 284–293, doi:10.1016/j.jhydrol.2011.10.039, 2012.

Serreze, M. C., Clark, M. P., Armstrong, R. L., McGinnis, D. A. and Pulwarty, R. S.: Characteristics of the western United States snowpack from snowpack telemetry (SNOTEL) data, Water Resour. Res., 35(7), 2145–2160, doi:10.1029/1999WR900090, 1999.

Sevruk, B., Ondrás, M. and Chvíla, B.: The WMO precipitation measurement intercomparisons, Atmospheric Research, 92(3), 376–380, doi:10.1016/j.atmosres.2009.01.016, 2009.

Strachan, S., Kelsey, E. P., Brown, R. F., Dascalu, S., Harris, F., Kent, G., Lyles, B., McCurdy, G., Slater, D. and Smith, K.: Filling the Data Gaps in Mountain Climate Observatories Through Advanced Technology, Refined Instrument Siting, and a Focus on Gradients, Mountain Research and Development, 36(4), 518–527, doi:10.1659/MRD-JOURNAL-D-16-00028.1, 2016.

Suding, K. N., Farrer, E. C., King, A. J., Kueppers, L. and Spasojevic, M. J.: Vegetation change at high elevation: scale dependence and interactive effects on Niwot Ridge, Plant Ecology & Diversity, 8(5–6), 713–725, doi:10.1080/17550874.2015.1010189, 2015.

Sugiura, K., Ohata, T. and Yang, D.: Catch characteristics of precipitation gauges in high-latitude regions with high winds, Journal of Hydrometeorology, 7(5), 984–994, 2006.

Sun, Q., Miao, C., Duan, Q., Ashouri, H., Sorooshian, S. and Hsu, K.: A Review of Global Precipitation Data Sets: Data Sources, Estimation, and Intercomparisons, Rev. Geophys., 56(1), 79–107, doi:10.1002/2017RG000574, 2018.

Thériault, J. M., Rasmussen, R., Ikeda, K. and Landolt, S.: Dependence of Snow Gauge Collection Efficiency on Snowflake Characteristics, J. Appl. Meteor. Climatol., 51(4), 745–762, doi:10.1175/JAMC-D-11-0116.1, 2012.

Thériault, J. M., Rasmussen, R., Petro, E., Trépanier, J.-Y., Colli, M. and Lanza, L. G.: Impact of Wind Direction, Wind Speed, and Particle Characteristics on the Collection Efficiency of the Double Fence Intercomparison Reference, J. Appl. Meteor. Climatol., 54(9), 1918–1930, doi:10.1175/JAMC-D-15-0034.1, 2015.

Tokay, A., Wolff, D. B. and Petersen, W. A.: Evaluation of the New Version of the Laser-Optical Disdrometer, OTT Parsivel ², J. Atmos. Oceanic Technol., 31(6), 1276–1288, doi:10.1175/JTECH-D-13-00174.1, 2014.

Westrick, K. J., Storck, P. and Mass, C. F.: Description and Evaluation of a Hydrometeorological Forecast System for Mountainous Watersheds, WEATHER AND FORECASTING, 17, 13, 2002.

Winstral, A., Marks, D. and Gurney, R.: Simulating wind-affected snow accumulations at catchment to basin scales, Advances in Water Resources, 55, 64–79, doi:10.1016/j.advwatres.2012.08.011, 2013.

Wolff, M. A., Isaksen, K., Petersen-Øverleir, A., Ødemark, K., Reitan, T. and Brækkan, R.: Derivation of a new continuous adjustment function for correcting wind-induced loss of solid precipitation: results of a Norwegian field study, Hydrol. Earth Syst. Sci., 19(2), 951–967, doi:10.5194/hess-19-951-2015, 2015.

Woods, C. P., Stoelinga, M. T. and Locatelli, J. D.: The IMPROVE-1 Storm of 1–2 February 2001. Part III: Sensitivity of a Mesoscale Model Simulation to the Representation of Snow Particle Types and Testing of a Bulk Microphysical Scheme with Snow Habit Prediction, J. Atmos. Sci., 64(11), 3927–3948, doi:10.1175/2007JAS2239.1, 2007.

Wu, C., Liu, X., Lin, Z., Rhoades, A. M., Ullrich, P. A., Zarzycki, C. M., Lu, Z. and Rahimi-Esfarjani, S. R.: Exploring a Variable-Resolution Approach for Simulating Regional Climate in the Rocky Mountain Region Using the VR-CESM: VR-CESM Simulation in the Rocky Mountains, J. Geophys. Res. Atmos., 122(20), 10,939-10,965, doi:10.1002/2017JD027008, 2017.

Yang, D., Goodison, B. E., Metcalfe, J. R., Golubev, V. S., Bates, R., Pangburn, T. and Hanson, C. L.: Accuracy of NWS 8″ Standard Nonrecording Precipitation Gauge: Results and Application of WMO Intercomparison, JOURNAL OF ATMOSPHERIC AND OCEANIC TECHNOLOGY, 15, 15, 1998a.

Yang, D., Goodison, B. E., Ishida, S. and Benson, C. S.: Adjustment of daily precipitation data at 10 climate stations in Alaska: Application of World Meteorological Organization

intercomparison results, Water Resour. Res., 34(2), 241–256, doi:10.1029/97WR02681, 1998b.

Yang, D., Goodison, B. E., Metcalfe, J. R., Louie, P., Leavesley, G., Emerson, D., Hanson, C. L., Golubev, V. S., Elomaa, E., Gunther, T., Pangburn, T., Kang, E. and Milkovic, J.: Quantification of precipitation measurement discontinuity induced by wind shields on national gauges, Water Resour. Res., 35(2), 491–508, doi:10.1029/1998WR900042, 1999.

Appendix A

A.1 JAGS model: rain

```
model{
  ## PRIORS
  b0 ~ dnorm(0, 0.01)
  b1 ~ dnorm(0, 0.01)
  b2 ~ dnorm(0, 0.01)
  b3 ~ dnorm(0, 0.01)
  b4 ~ dnorm(0, 0.01)
  b24 ~ dnorm(0, 0.1)
  tauy ~ dgamma(0.001,0.001)
  tauxr_ws ~ dunif(0.3,0.4)
  tauxr_int ~ dunif(0.85,0.95)
  tauxr_dur ~ dunif(0.8,0.9)
  tauxr_par ~ dunif(0.8,0.9)
```

```
  ## LIKELIHOOD
  for(i in 1 : nData ) {
    truexr_ws[i] ~ dgamma(5.738079,0.1603397)
    xr_ws[i] ~ dnorm(truexr_ws[i], tauxr_ws)
    truexr_int[i] ~ dgamma(0.2165204,1.947229)
    xr_int[i] ~ dnorm(truexr_int[i], tauxr_int)
    truexr_dur[i] ~ dgamma(0.4173668,1.298814)
    xr_dur[i] ~ dnorm(truexr_dur[i], tauxr_dur)
    truexr_par[i] ~ dgamma(0.1362195, 2.540766)
    xr_par[i] ~ dnorm(truexr_par[i], tauxr_par)
    yr[i] ~ dt(y.hat[i], tauy, 1)
    y.hat[i] <- b0 + b1 * truexr_par[i] + b2 * truexr_int[i] +
      b3 * truexr_dur[i] + b4 * truexr_ws[i] +
      b24 * truexr_int[i] * truexr_ws[i]}}
```

Figure A.1. JAGS model formulation for rain precipitation type. b0 = intercept coefficient, b1 = total particles coefficient, b2 = intensity coefficient, b3 = duration coefficient, b4 = wind speed coefficient, b24 = intensity * wind speed interaction coefficient, tauy = vauge precision parameter for T distribution, tauxr _ws = uniform standard deviation hyperprior for wind speed, tauxr _int = uniform standard deviation hyperprior for intensity, tauxr _dur = uniform standard deviation hyperprior for duration, tauxr _par = uniform standard deviation hyperprior for total particles ,nData = length of predictions, truexr _ws = sampling of wind speed from gamma distribution, xr_ws = wind speed model variable, truexr _int = sampling of intensity from gamma distribution, xr _int = intensity model variable, truexr _dur = sampling of duration from gamma distribution, xr_dur = duration model variable, truexr_par = sampling of total particles from gamma distribution, xr_par = total particles model variable, yr = sampling of CRN-Met from Cauchy distribution, y.hat = the predicted difference (CRN-Met).

A.2 JAGS model: mixed

```
model{
 ## PRIORS
 b0 ~ dnorm(0, 0.01)
 b1 ~ dnorm(0, 0.01)
 b2 ~ dnorm(0, 0.01)
 b3 ~ dnorm(0, 0.01)
 b4 ~ dnorm(0, 0.01)
 tauy ~ dgamma(0.001,0.001)
 tauxm_ws ~ dunif(0.4,0.5)
 tauxm_int ~ dunif(0.85,0.95)
 tauxm_dur ~ dunif(0.8,0.9)
 tauxm_par ~ dunif(0.8,0.9)
```

```
 ## LIKELIHOOD
 for(i in 1 : nData ) {
  truexm_ws[i] ~ dgamma(2.580335,0.3272983)
  xm_ws[i] ~ dnorm(truexm_ws[i], tauxm_ws)
  truexm_int[i] ~ dgamma(0.2809226,1.664394)
  xm_int[i] ~ dnorm(truexm_int[i], tauxm_int)
  truexm_dur[i] ~ dgamma(0.56958348,1.054849)
  xm_dur[i] ~ dnorm(truexm_dur[i], tauxm_dur)
  truexm_par[i] ~ dgamma(0.4767221, 1.189062)
  xm_par[i] ~ dnorm(truexm_par[i], tauxm_par)
  ym[i] ~ dt(y.hat[i], tauy, 1)
  y.hat[i] <- b0 + b1 * truexm_par[i] + b2 * truexm_int[i] +
    b3 * truexm_dur[i] + b4 * truexm_ws[i]}}
```

Figure A.2. JAGS model formulation for mixed precipitation type. b0 = intercept coefficient, b1 = total particles coefficient, b2 = intensity coefficient, b3 = duration coefficient, b4 = wind speed coefficient, tauy = vauge precision parameter for T distribution, tauxm _ws = uniform standard deviation hyperprior for wind speed, tauxm _int = uniform standard deviation hyperprior for intensity, tauxm _dur = uniform standard deviation hyperprior for duration, tauxm _par = uniform standard deviation hyperprior for total particles ,nData = length of predictions, truexm _ws = sampling of wind speed from gamma distribution, xm_ws = wind speed model variable, truexm _int = sampling of intensity from gamma distribution, xm _int = intensity model variable, truexm _dur = sampling of duration from gamma distribution, xm_dur = duration model variable, truexm_par = sampling of total particles from gamma distribution, xm_par = total particles model variable, yr = sampling of CRN-Met from Cauchy distribution, y.hat = the predicted difference (CRN-Met).

A.3 JAGS model: snow

```
model{
  ## PRIORS
  b0 ~ dnorm(0, 3)
  b1 ~ dnorm(1.5, 3)
  b2 ~ dnorm(2, 5)
  b3 ~ dnorm(0, 2)
  b4 ~ dnorm(0, 3)
  b24 ~ dnorm(-2.5, 6)
  b12 ~ dnorm(0, 1)
  tauy ~ dgamma(0.001,0.001)
  tauxs_ved ~ dunif(0.2,0.3)
  tauxs_int ~ dunif(0.73,1.3)
  tauxs_dur ~ dunif(0.6,0.7)
  tauxs_par ~ dunif(0.65,0.75)
```

```
  ## LIKELIHOOD
  for(i in 1 : nData ) {
    truexs_ved[i] ~ dgamma(17.4844,0.05548508)
    xs_ved[i] ~ dnorm(truexs_ved[i], tauxs_ved)
    truexs_int[i] ~ dgamma(0.6330469,0.9825011)
    xs_int[i] ~ dnorm(truexs_int[i], tauxs_int)
    truexs_dur[i] ~ dgamma(1.456773,0.5277571)
    xs_dur[i] ~ dnorm(truexs_dur[i], tauxs_dur)
    truexs_par[i] ~ dgamma(0.9777428, 0.7181736)
    xs_par[i] ~ dnorm(truexs_par[i], tauxs_par)
    ys[i] ~ dt(y.hat[i], tauy, 1)
    y.hat[i] <- b0 + b1 * truexs_int[i] + b2 * truexs_par[i] +
      b3 * truexs_dur[i] + b4 * truexs_ved[i] +
      b24 * truexs_par[i] * truexs_ved[i] +
      b12 * truexs_int[i] * truexs_par[i]}}
```

Figure A.3. JAGS model formulation for snow precipitation type. b0 = intercept coefficient, b1 = intensity coefficient, b2 = total particles coefficient, b3 = duration coefficient, b4 = VED coefficient, b24 = total particles*VED interaction coefficient, b12 = intensity*total particles interaction coefficient, tauy = vague precision parameter for T distribution, tauxs_ved = uniform standard deviation hyperprior for VED, tauxs_int = uniform standard deviation hyperprior for intensity, tauxs _dur = uniform standard deviation hyperprior for duration, tauxs _par = uniform standard deviation hyperprior for total particles ,nData = length of predictions, truexs_ved = sampling of VED from gamma distribution, xs_ved = VED model variable, truexs_int = sampling of intensity from gamma distribution, xs_int = intensity model variable, truexs_dur = sampling of duration from gamma distribution, xs_dur = duration model variable, truexs_par = sampling of total particles from gamma distribution, xs_par = total particles model variable, ys = sampling of CRN-Met from Cauchy distribution, y.hat = the predicted difference (CRN-Met).